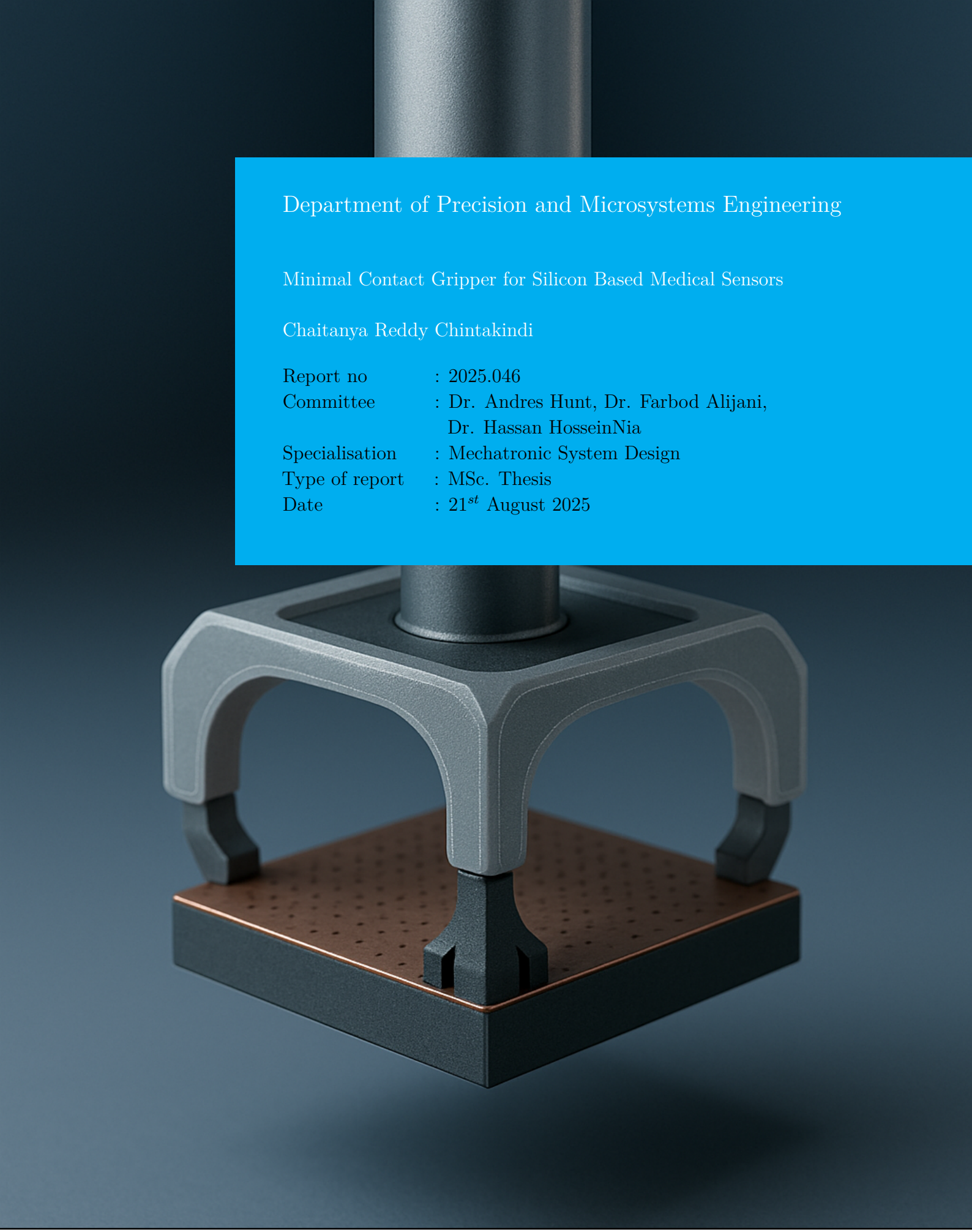

Department of Precision and Microsystems Engineering

Minimal Contact Gripper for Silicon Based Medical Sensors

Chaitanya Reddy Chintakindi

Report no	: 2025.046
Committee	: Dr. Andres Hunt, Dr. Farbod Alijani, Dr. Hassan HosseinNia
Specialisation	: Mechatronic System Design
Type of report	: MSc. Thesis
Date	: 21^{st} August 2025

TU Delft Delft University of Technology

Challenge the future

Minimal Contact Gripper for Silicon Based Medical Sensors

by

Chaitanya Reddy Chintakindi

to obtain the degree of Master of Science

at the Delft University of Technology,

to be defended publicly on Thursday August 21, 2025 at 09:30 AM.

Student number:	5690617	
Thesis committee:	Dr. Andres Hunt	TU Delft
	Dr. Farbod Alijani	TU Delft
	Dr. Hassan HosseinNia Kani	TU Delft

TU Delft

Preface

I would like to express my sincere gratitude to Dr. Farbod Alijani for giving me the opportunity to work on this topic, and to Dr. Andres Hunt for his invaluable guidance in approaching and structuring the thesis problem. I am also thankful to the PME laboratory staff, namely Bradley and Gideon for their timely assistance and support during the experimental work.

My heartfelt thanks go to the friends I have made during my master's journey, whose constant encouragement and companionship have been a source of motivation throughout this period.

This research topic has allowed me to view the concept of gripping in a completely new light, introducing me to the fascinating domain of robotic grasping, an area that quickly became a deep and engaging rabbit hole for exploration. Beyond the technical knowledge gained, my master's journey has been a profound learning experience that has shaped my understanding not only of engineering, but also of life itself.

Chaitanya Reddy Chintakindi
Delft, August 2025

Abstract

The precise and damage-free manipulation of fragile chips such as sensors, MEMS devices, or other micro-fabricated components with surface-bound structures demands grippers that can operate reliably within highly constrained assembly environments. These chips often feature delicate surface components that preclude traditional gripping strategies, especially in contexts where clearances are limited to sub-millimeter levels. This work develops and experimentally validates a generalizable framework called the Grasp Analysis Methodology (GAM) that combines Grasp Wrench Space (GWS) analysis with classical force distribution theory to support the design and evaluation of grippers for such applications. The framework is applied to three distinct gripper configurations: an industry-standard surface grasp gripper, a three-point gripper derived from the decomposition of a typical edge-based industrial gripper, and a four-point corner-supported design. Grasp quality is assessed using GWS metrics, which characterize each configuration's ability to resist external disturbances through its wrench space properties. Concurrently, the mechanical loading experienced by the chip during grasping is estimated using plate theory to understand stress concentrations and risk of damage. To validate these analytical results and hence the gripper designs, a series of experimental tests is conducted. Pull tests evaluate disturbance resistance, while placement trials examine the gripper's ability to preserve the chip's orientation from pick up to placement, a critical requirement in precision assembly tasks. Unlike most academic gripper designs, which are either unvalidated or unconstrained, this study emphasizes real-world feasibility by testing under a spatial clearance of just $0.5mm$. The findings demonstrate that the proposed GWS-Force strategy under the developed GAM workflow offers a robust basis for evaluating and optimizing chip grippers in constrained, high-precision environments.

Contents

List of Figures

List of Tables

1

Introduction

1.1. Scope

This thesis performs the design and evaluation of novel vacuum-actuated grippers for handling square, silicon-based MEMS chips with sensitive top surfaces and a defined no-contact central region. A detailed analytical grasp analysis methodology is developed to evaluate multiple grasp configurations, assessed under tight clearance constraints representative of precision assembly environments. The analysis is restricted to quasi-static conditions and, in this work, applied to planar chips with a known center of mass. Experimental validation is performed to ensure the developed methodology's and gripper design's operational reliability.

The framework developed here addresses two key gaps in existing literature, i.e. the lack of quantitative grasp quality evaluation using GWS in experimentally tested grippers, and the absence of testing under sub-millimeter spatial constraints where objects are positioned close together. While demonstrated on planar MEMS chips, the methodology is applicable to other pick and place scenarios, including those involving complex or non-planar objects, provided the object's geometry and center of mass are known.

1.2. Background and Motivation

Silicon MEMS chips have now transformed into ubiquitous inertial, optical, and biochemical sensors [1, 2]. In the rapidly evolving semiconductor industry, the miniaturisation of components and the integration of sensitive microstructures on silicon MEMS chips have introduced new challenges in high-precision assembly. Conventional pick-and-place strategies must hence be re-evaluated, particularly in Micro Electro-Mechanical Systems (MEMS) applications where on-chip elements such as suspended membranes, bond pads, or microfluidic interfaces are highly vulnerable. Therefore, contact-based handling solutions can result in damage or yield loss of these chips [3, 4, 5, 6]. This motivates the development of gripper designs that ensure safe and precise manipulation.

SoundCell's *MelodyOne* antibiotic-susceptibility platform integrates large arrays of graphene drum membranes on a silicon-chip to detect the nanomotion of single bacteria within one hour [7, 8] (see Figure 1.1a-1.1b). The extreme fragility of these suspended membranes highlights the need for grippers that never touch the top surface and impose minimal edge stress during assembly. Analyzing stresses at the edges is hence pivotal as they can create micro-cracks leading to die fractures, which are a primary cause of yield loss in individual wafers (see Figure 1.2).

Several authors have proposed methods for gripping sensitive objects using a range of bernoulli-based and acoustic technologies[9, 10, 11, 12]. These approaches demonstrate the potential of non-contact handling techniques to minimize mechanical stress and surface contamination. Nevertheless, limitations remain in terms of geometrical constraints, force control, and adaptability to varying object geometries. Out of these, geometrical constraints are the most critical yet underexplored considerations for the gripping of sensitive silicon chips in the modern semiconductor industry. These research gaps are analyzed and elaborated in the following section.

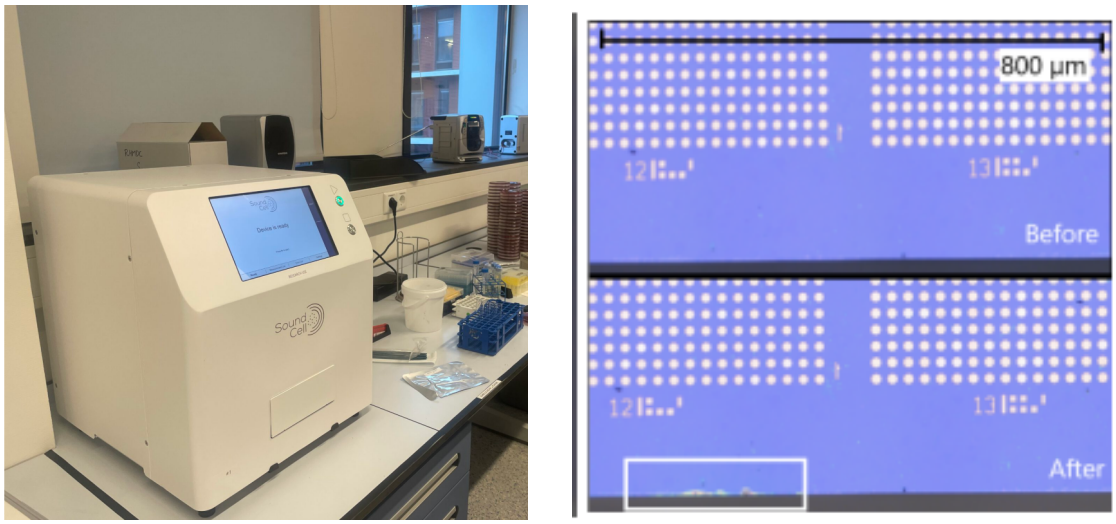

(a) MelodyOne platform developed by SoundCell B.V. [7]

(b) The medical sensor developed by Roslon et al. [8]

Figure 1.1: Medical device developed by SoundCell B.V. for rapid antimicrobial susceptibility testing

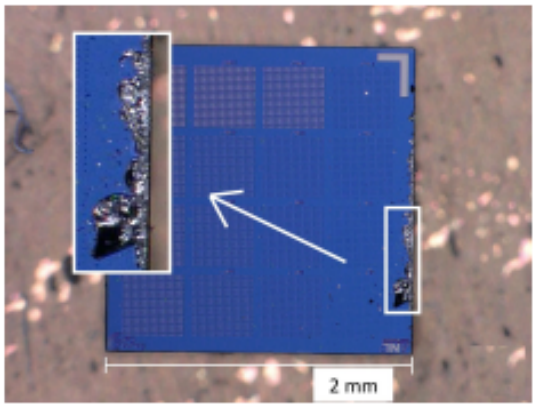

Figure 1.2: Edge damage caused during pick up operation; Image adapted from the Bachelors End Project of student group with Dr. Peter Steeneken in hte DMN group

1.2.1. Critical Research Gaps

Critical gaps for sensitive MEMS chip grippers to be addressed in this thesis are identified as follows.

1. **Lack of constrained gripping environments:** Recent advances in gripper technologies have introduced a wide range of gripping mechanisms, including electrostatic [13],, piezoelectric [14], and soft-robotic approaches [15]. However, most of these grippers are tested in controlled laboratory conditions, typically on open benchtops, and are rarely evaluated within the constrained geometries often found in industrial MEMS packaging environments. Hence, this field lacks a non-invasive gripping approach that:
    - Eliminates or minimises contact with sensitive on-chip structures.
    - Localises mechanical stresses away from fragile die edges.
    - Functions reliably within the space and placement constraints of MEMS production environments.
2. **Lack of proper testing:** Despite promising performance at the prototype level, a clear gap remains in the development of a rigorously validated gripping approach that can meet the operational requirements in terms of pick-and-place operations under tight geometrical constraints

[16][17][18][19].

1.3. Thesis Objectives

Traditional pick and place tools are not well-suited for handling silicon-chips that have delicate surface structures and are prone to edge damage. Therefore, to address the above-mentioned research gaps, a new gripping approach is needed that avoids damaging sensitive areas while still working within the size and accuracy limits of semiconductor assembly systems. The thesis objectives below capture this challenge and form the foundation for the work that follows.

Overall objective: *Design and validate grippers with minimal contact, alongside formulating a novel gripper design workflow, i.e. the Grasp Analysis Methodology (GAM), while retaining placement precision on a sub-millimeter scale during automated pick and place operations of silicon-based graphene medical sensors.*

- **Sub-objective 1:** To strategically place gripper contact points to ensure maximum free top surface area for sensitive on-chip components.

  This is to explore the spatial positioning of contact interfaces to avoid interference with fragile functional areas while ensuring sufficient mechanical stability during gripping.

- **Sub-objective 2:** To balance gripper contact force distributions for mitigating edge damage.

  This sub-objective is for investigating how gripper geometry can be designed to constrain contact forces within safe regions away from fragile chip edges by imposing predefined mechanical boundaries. Rather than relying on compliance or adaptive deformation, the approach focuses on controlling contact locations and limiting stress concentrations through geometric design choices.

- **Sub-objective 3:** To validate the chip's placement constraints by the designed grippers.

  This is to experimentally evaluate whether the proposed grippers perform within the precision, repeatability and clearance limits imposed by automated assembly systems.

To address these problems, this work aims to design and evaluate gripper mechanisms tailored for the safe and precise pick and place handling of a specialized silicon-based medical sensor developed by SoundCell B.V. for integration into automated diagnostic platforms. For this purpose, a novel gripper design framework is proposed, called the Grasp Analysis Methodology (GAM), which can also be extended to similar gripper design problems. The research investigates design strategies that avoid contact with functional top-side regions, constrain contact to structurally safe areas, and meet stringent spatial and placement constraints associated with pick-and-place operations of delicate silicon sensors. By combining analytical modeling through grasp analysis and experimental validation, this work aims to deliver a non-invasive handling approach suitable for scalable medical device assembly.

1.4. Thesis Outline

An overview of the structure of this thesis is as follows:

- **chapter 2 - Literature Review and Preliminaries** provides a comprehensive literature review of current pick-and-place gripper technologies, alongside specific gripper analysis preliminaries.This chapter also discusses their suitability for handling fragile silicon chips and concludes with a motivated concept selection based on performance limitations and associated trade-offs.
- **chapter 3 - Grasp Analysis Methodology and Gripper Design** details the analytical formulation of the gripping techniques. This includes the definition of design constraints, the development of a wrench-based grasp analysis, and a force distribution study to evaluate how the gripper interacts with the chip. Apart from developing the novel gripper designs, the Grasp Analysis Methodology (GAM) is simultaneously formulated.
- **chapter 4 - Experimental Validation and Discussion** presents the experimental validation of the proposed grippers. Performance testing is conducted to compare analytical predictions with real-world behavior, focusing on placement accuracy, slippage resistance, and chip integrity post-handling.

- **chapter 5 - Conclusion** summarizes the major findings of the research, reflects on the design and analysis methodology, and outlines opportunities for future work.

2

Literature Review and Theoretical Background

Building on the foundational concepts and objectives established in chapter 1, this chapter examines the body of existing work and the theoretical tools that define gripper design. Having defined the need for a non-invasive, high precision handling strategy for silicon-based medical sensors, this chapter now reviews the state of the art in semiconductor pick and place technologies, identifies their key advantages and shortcomings, and selects the most promising approaches for detailed analysis. The chapter then introduces the core mathematical framework, like grasp wrench space and force closure theory that guides the quantitative comparison of alternative gripper configurations. Specifically, section 2.1 surveys a range of mechanical, vacuum, magnetic, electroadhesive, Bernoulli, and acoustic grippers, section 2.2 presents the rationale for choosing a modified vacuum grip, and section 2.3 provides the fundamentals of friction cones, wrench space modelling, and grasp quality metrics. Together, these elements establish the theoretical background necessary to evaluate the three candidate grasps in chapter 3.

2.1. State of the Art

This section provides a concise overview of gripper types used in semiconductor pick and place applications. It outlines the working principles, strengths, and limitations of established and emerging gripper types, namely mechanical, vacuum, magnetic, electroadhesive, Bernoulli, and acoustic systems, drawing from both academic research and industrial practice.

- **Mechanical grippers:** They use direct contact, often through jaws or compliant fingers, to grasp chips and are well suited to rigid components in tasks requiring micrometer accuracy, such as MEMS assembly. Xu et al. [20] propose a structured selection based on CAD models, enhancing automation planning. Llewellyn-Evans et al. [21] evaluated configurations for micro-wire assembly, focusing on stability and centring.

- **Vacuum grippers:** They lift flat components using suction and are the mainstream industrial solution for wafers and dies. Baek and Kim [22] introduced real-time suction detection using Venturi sensors, improving reliability. Yoo et al. [23] developed compliant suction cups compensating for tilt errors up to 60°, while Song et al. [24] showed soft membrane suction improves grip on non-planar surfaces.

- **Magnetic grippers:** These magnetic grippers use external magnetic fields to handle chips with ferromagnetic coatings, enabling non-contact placement. Lee et al. [25] demonstrated self-alignment and vertical assembly of nickel-coated microchips without mechanical contact, followed

by wire bonding.

- **Electroadhesive grippers:** Electrostatic grippers use forces between electrode pads and the component surface, often with dielectric layers. EA stamps have manipulated LED chiplets as small as 170 μm with only 30 V applied [26]. Persson and Guo [27] analysed electrode geometry and surface roughness affecting adhesion. More recent soft metamaterial EA grippers improve payload release tuning and grip across diverse surfaces [28]. EA methods excel for delicate, flexible, or porous components [29].

- **Bernoulli grippers:** In order to lift flat surfaces without making contact, vacuum-based grippers create low-pressure zones through high-velocity radial airflow. CFD studies optimize the nozzle geometry and gap parameters to increase lifting force and efficiency [30, 31]. Tests on thin or curled silicon wafers showed that lift occurs but with limitations: only specific gripper models (e.g. B20) could handle certain wafer shapes reliably [11]. They are used in wafer-level handling but require careful control of distance and pressure.

- **Acoustic grippers:** Acoustic grippers, including standing-wave and near-field levitation systems, offer contactless manipulation suitable for micro objects. Standing-wave setups using transducer-reflector pairs can trap and move particles, with phase control enabling vertical movement and release [32, 33]. Near-field levitation systems have demonstrated contactless pick and place of millimetric objects with self-centring and orientation control [34]. Such systems remain in academic stages but hold promise for ultra-clean, precise chip manipulation.

Table 2.1 gives a brief comparison of six common gripper types used for handling semiconductor chips. It shows their contact mode, main strengths, and key limitations.

Gripper Type	Contact Mode	Key Strengths	Primary Limitations
Mechanical	Direct contact	High gripping force; precise actuation control	Potential for mechanical damage or contamination
Vacuum	Soft contact	Fast, clean transfer; quick assembly time	Sensitive to surface leakage and roughness
Magnetic	Direct contact	Clean, self-aligning holding	Requires ferromagnetic material on the object
Electroadhesion	Direct contact	Gentle; conforms to textured or uneven surfaces	Limited force capacity; requires high-voltage supply
Bernoulli	Non-contact	Non-contact lifting of flat, rigid objects	Limited to planar parts; unstable in turbulent environments
Acoustic	Non-contact	Precise, ultra-delicate manipulation	Low throughput; limited industrial adoption

Table 2.1: Comparison of gripper technologies for semiconductor chip handling.

Mechanical and vacuum grippers are well established in industrial semiconductor assembly, while magnetic, electroadhesive, Bernoulli, and acoustic methods emerge in research as contactless or low-contact alternatives advantageous for fragile, small, or contamination-sensitive components.

2.2. Adoption of Vacuum-Based Gripper

Based on a comparative analysis of the available gripper technologies, vacuum based gripping emerged as the most viable solution for the pick and place operation of silicon MEMS chips with sensitive on surface structures. Although mechanical gripper offers robust holding capabilities, they pose a higher risk of surface contamination or stress concentration at the die edges. Magnetic grippers are inherently not compatible with silicon chips. Electroadhesion gripper can cause damage to the on surface chip components through charge Acoustic grippers, though promising in non-contact manipulation, are largely in the proof of concept stage and often require complex control or environmental constraints not readily compatible with high throughput industrial integration.

Vacuum grippers, by contrast, offer a well established, high-speed platform with a relatively simple implementation footprint. Their compatibility with planar surfaces and ease of integration into automated assembly lines make them particularly attractive for MEMS-level packaging. However, conventional suction cups can obscure sensitive surface regions or induce slippage and misalignment under rapid actuation[35].

To address these limitations, the proposed concept incorporates a modified vacuum based gripper augmented with passive mechanical stoppers. These stoppers serve to localise contact at predefined non-functional edge regions, thereby protecting surface-mounted structures from unintended contact while also helping to constrain lateral chip motion during placement. This hybrid approach leverages the practicality of vacuum actuation while mitigating its primary drawbacks, offering a balance between delicacy, reliability, and industrial feasibility.

2.3. Preliminaries for Grasp Modelling

This section presents the theoretical foundations for grasp modelling, starting with closure types and proceeding to wrench space representation and closure criteria. Then it describes analytical contact models and friction cones, followed by the formulation of the grasp matrix and wrench-based analysis. Finally, it introduces grasp quality metrics that form the basis for the evaluation pipeline used in this work.

2.3.1. Grasp Closure Types

In robotics, a grasp is the set of contacts that allows a manipulator to control the posture of an object [36, 37]. We use the following terms.

- **Form closure:** Form closure is reached by a grasp when all conceivable tiny motions of the item are completely restricted by the enforced geometric restrictions at the contact points, regardless of the direction or size of any externally induced disturbance. This condition does not require friction and is dependent only on the kinematics and spatial arrangement of the contacts. [36].

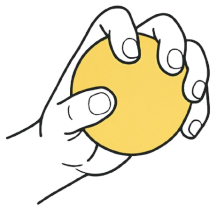

Figure 2.1: Form Closure of an object

- **Force closure:** A grab achieves force closure when the available contact forces balance an arbitrary external disturbance operating on the object. To minimise the number of necessary contacts, this condition utilises friction to enhance constraint capability.
- **Partial form closure:** This condition arises when the geometric constraints eliminate only a subset of the object's degrees of freedom, leaving certain motions (such as specific translations

or rotations) unconstrained. Although complete immobilisation is not achieved, residual mobility is often acceptable for tasks where only task-relevant disturbances need to be prevented.

- **Partial force closure:** This refers to a grasp configuration that can resist a defined subset of possible external disturbances, but not all. The admissible contact force set is therefore sufficient only for counteracting anticipated disturbance patterns during the intended operation, rather than for providing complete resistance to arbitrary disturbances.

2.3.2. Wrench Space and Closure Criteria

To evaluate closure conditions quantitatively, each contact with friction is modelled by a *friction cone* representing the set of admissible force directions. The combination of forces and associated torques at each contact yields a set of wrenches, which collectively form a convex region in the six-dimensional wrench space [36, 38]. A grasp is classified as having closure if the origin lies strictly within the interior of the convex hull of these admissible wrenches.

Closure strategy chosen in this work:

Given the no-contact central regions and sub millimetre spatial constraints of the target chips, the designs in this work are *partial form closure* as verified through Grasp Wrench Space (GWS) analysis.

The subsequent sections expand upon these theoretical foundations by constructing analytical tools for quantitative grasp assessment.

2.3.3. Analytical Grasp Modeling through Wrench Analysis

Contact Models:

1. **Point Contact without Friction (PWoF)**: A widely accepted initial approach in contact mechanics is to assume that the interface between two bodies is entirely frictionless. While no physical contact is ever truly free of friction, this assumption is informative in scenarios where friction is minimal or the surface traction varies substantially. Consequently, frictionless contact analysis is often employed as a foundational investigation to gain insight into the basic principles of grasp mechanics. In a frictionless contact, the force transmitted between the bodies is restricted to act along the normal direction of the contact surfaces. Mathematically, this is described by

$$\mathbf{F}_i = F_{n_i}\,\mathbf{n}_i, \quad F_{n_i} \geq 0. \tag{2.1}$$

where $F_{n_i} \geq 0$ is a nonnegative scalar, and $\mathbf{n}_i$ is the inward-pointing unit normal on body B at the contact point. The constraint $F_{n_i} \geq 0$ reflects the fact that a rigid body can only exert a pushing (compressive) force at the contact; it cannot pull in tension without friction.

Friction Cone Representation: The set of all feasible contact forces for a frictionless point contact can be written as

$$C_i = \left\{\mathbf{F}_i \in \mathbb{R}^3 : \mathbf{F}_i = F_{n_i}\,\mathbf{n}_i,\, F_{n_i} \geq 0\right\}, \tag{2.2}$$

which reduces to $\mathbf{F}_i \in \mathbb{R}^2$ in planar (2D) analyses. Geometrically, C_i forms a half-line (or a one-dimensional cone) originating at the contact location and directed along the inward normal vector. Essentially, only the normal force f_z can be exerted between the contacting bodies, and this normal component must satisfy $f_z \geq 0$.

2. **Point Contact with Friction**: Let the superscripts F_i^{t1}, F_i^{t2}, and F_i^n denote the tangential and normal components of the contact force $\mathbf{F}_i$ with respect to the i-th contact frame. Specifically, these components are given by

$$(F_i^{t1}, F_i^{t2}) = (\mathbf{F}_i \cdot \mathbf{t}_1,\, \mathbf{F}_i \cdot \mathbf{t}_2), \quad F_i^n = \mathbf{F}_i \cdot \mathbf{n}_i, \tag{2.3}$$

where $\{\mathbf{t}_1, \mathbf{t}_2, \mathbf{n}_i\}$ constitute the coordinate axes of the i-th contact frame, with $\mathbf{n}_i$ pointing inward toward body B. Under the static Coulomb friction model, the contact (or rigid body) can exert only a unilateral (pushing) force along the inward normal, so $F_i^n \geq 0$. Due to friction, the contact also gains the ability to apply tangential forces (F_i^{t1}, F_i^{t2}). However, if these tangential components become too large, the contact will begin sliding over the object's surface.

According to the Coulomb friction model, there will be no slip at the contact provided that

$$|F_i \cdot \mathbf{t}_1 + F_i \cdot \mathbf{t}_2| \leq \mu_i \cdot F_i^n. \tag{2.4}$$

where μ_i is the coefficient of friction associated with the i-th contact. As soon as the tangential force exceeds this bound, sliding occurs, and the magnitude of the tangential reaction force satisfies

$$|F_i \cdot \mathbf{t}_1 + F_i \cdot \mathbf{t}_2| = \mu_i \cdot F_i^n. \tag{2.5}$$

Friction Cone Representation: The friction cone defines feasible frictional forces at a contact:

$$C_i = \left\{ \mathbf{F}_i \in \mathbb{R}^3 : \mathbf{F}_i \cdot \mathbf{n}_i \geq 0, \quad (\mathbf{F}_i \cdot \mathbf{t_1}_i)^2 + (\mathbf{F}_i \cdot \mathbf{t_2}_i)^2 \leq \mu_i \left(\mathbf{F}_i \cdot \mathbf{n}_i\right) \right\}. \tag{2.6}$$

Geometrically, C_i forms a convex cone whose vertex is the contact point, with a half-angle $\beta_i = \tan^{-1}(\mu_i)$. Provided the applied force lies within this cone, the grasp remains stable.

Subsequent analyses employ these detailed contact mechanics to construct grasp matrices, perform wrench space analyses, and evaluate grasp robustness quantitatively.

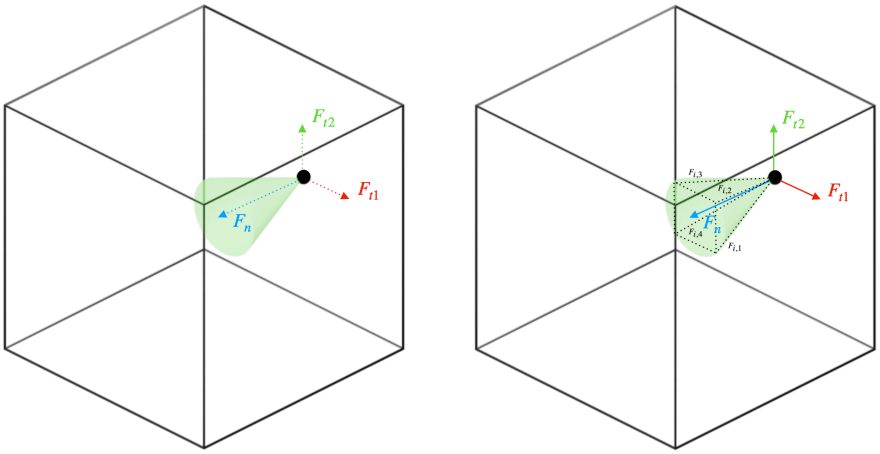

(a) Friction cone for a spatial grasp **(b)** Discretized friction cone for a spatial grasp

Figure 2.2: Depiction of friction cone and the subsequent discretized form for a single contact for a spatial frictional grasp

Grasp Matrix and Wrench Cones

Formally, a wrench combines a linear force $F \in \mathbb{R}^3$ and associated torque $\tau \in \mathbb{R}^3$. A wrench generated by a contact force F_i at position x_i relative to the object's reference point p is mathematically expressed as:

$$w_i = \begin{bmatrix} F_i \\ (x_i - p) \times F_i \end{bmatrix} \in \mathbb{R}^6. \tag{2.7}$$

For multiple contacts, the net wrench is the sum of individual wrenches, captured through the grasp matrix G:

$$w_{\text{total}} = G \cdot F = \sum_{i=1}^{n} G_i F_i, \tag{2.8}$$

where G_i is the grasp mapping for each contact:

$$G = [G_1 \quad G_2 \quad \dots \quad G_n], \quad \text{with} \quad G_i = \begin{bmatrix} I \\ S(x_i - p) \end{bmatrix}. \tag{2.9}$$

Here, $S(x_i - p)$ is the skew-symmetric matrix corresponding to the vector $x_i - p$.

Contact and Net Wrench Cones Consider an object B positioned at q_0, contacted by contact bodies $O_1, \ldots, O_k$. The i-th contact wrench cone W_i is defined as the set of all possible wrenches that the i-th contact can apply to the object:

$$W_i = \{(f_i, x_i \times F_i) \in T^*_{q_0}\mathbb{R}^m : F_i \in C_i\}, \tag{2.10}$$

where C_i denotes the friction cone at the i-th contact, as detailed in subsection 3.4.1. Geometrically, W_i forms a convex cone with its vertex at the wrench space origin. For planar frictional contacts, this cone manifests as a two dimensional sector bounded by forces at the friction cone edges.

The net wrench set W considered in this analysis is defined as the union of the individual wrench cones at each contact point:

$$W = \bigcup_{i=1}^{k} W_i, \tag{2.11}$$

where each W_i represents the feasible wrenches that can be applied by the i-th contact under local friction and force constraints. This union based representation allows for a conservative yet insightful evaluation of the directions in which the grasp can resist disturbances.

Practical Implications for System Integration The wrench based formulation is particularly valuable in gripper design due to its direct relationship with system level requirements, especially the need to maintain static equilibrium during manipulation:

$$w_{\text{external}} + \sum_{i=1}^{n} G_i F_i = 0, \tag{2.12}$$

where G_i represents the grasp matrices derived earlier in Section 3.4, and w_i are the wrenches applied at each contact point. This expression forms the foundation for evaluating grasp feasibility, stability, and performance under external loads.

Beyond theoretical analysis, this equilibrium formulation enables several practical design insights and integration strategies, as outlined below:

- **Grasp Stability Assessment:** By leveraging wrench-based analyses, designers quantitatively assess grasp quality. Factors such as resistance to external wrenches and sensitivity to positional errors are evaluated to identify optimal contact placements and configurations, directly informing offline grasp planning and real-time grasp adjustments [39].

- **Actuation System Specifications:** Detailed grasp analyses guide actuator specifications, ensuring the gripper can provide adequate force ranges, precision, and response times. Simulations of grasp scenarios determine actuator capabilities necessary for stable handling without excessive force that might damage delicate objects [40].

- **Adaptive and Underactuated Designs:** Understanding wrench spaces and grasp stability aids in designing adaptive and underactuated grippers. Analysis of contact configurations guides the creation of mechanisms capable of passively adapting to varying object geometries, thereby enhancing versatility and robustness in manipulation tasks [41].

2.3.4. Grasp Quality

Once the number of contact points required to achieve partial immobilization is determined, the next step is to select a grasp configuration suitable for the pick and place operation of the chip. For an n-contact grasp on a square chip, there are infinitely many ways the object can be held, but not all grasps are equally robust. To compare and select between grasp configurations, it is necessary to quantify *how good* a grasp is in resisting disturbances. This is done through a **grasp quality function**.Physically, it assesses the grasp's security in the presence of real-world limitations like actuator force limits and friction limits.

Bounded Contact Forces

In practical robotic systems, contact forces are constrained by actuator limitations and surface friction. To account for these, each normal contact force component f_i^n is normalized within the unit interval:

$$0 \leq f_i^n \leq 1 \quad \text{for } i = 1, \ldots, k. \tag{2.13}$$

Each friction cone C_i imposes constraints on the tangential force components:

$$(f_i^s)^2 + (f_i^t)^2 \leq \mu_i f_i^n \quad \text{for } i = 1, \ldots, k, \tag{2.14}$$

where μ_i is the friction coefficient at contact point x_i.

These constraints result in a **bounded contact wrench cone** at each contact point, denoted by $\mathcal{W}_i$:

$$\mathcal{W}_i = \left\{ \mathbf{w}_i = G_i \mathbf{f}_i \;\middle|\; 0 \leq f_i^n \leq 1,\ (f_i^s)^2 + (f_i^t)^2 \leq \mu_i f_i^n \right\}, \tag{2.15}$$

where G_i is the i-th submatrix of the grasp matrix $G(q_0)$. Each $\mathcal{W}_i$ represents the set of wrenches that can be applied by a single contact point under both friction and actuation limits.

Grasp Quality Evaluation Pipeline

The evaluation of grasp quality in this work proceeds in three main steps:

1. **Convex Hull:** For each contact, the feasible wrench set $\mathcal{W}_i$ is computed using the bounded contact forces. The convex hull of these wrenches captures all possible net wrenches that contact can generate. Formally, given a finite set of vectors $\{v_1, v_2, \ldots, v_n\}$, their convex hull is defined as:

$$\text{co}(v_1, \ldots, v_n) = \left\{ \sum_{i=1}^{n} \alpha_i v_i \;\middle|\; \alpha_i \geq 0,\ \sum_{i=1}^{n} \alpha_i = 1 \right\}. \tag{2.16}$$

   Geometrically, the convex hull can be visualized as the shape formed by stretching a tight elastic band around the outermost points in the set , resulting in the smallest convex shape that encloses them, as shown in Figure 2.3. In two dimensions, this resembles a polygon; in three dimensions, a polytype.

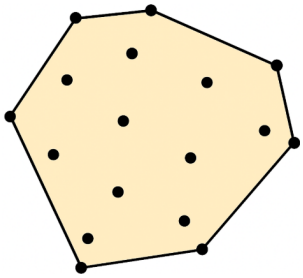

Figure 2.3: Depiction of a convex hull

2. **Grasp Wrench Space (GWS):** The convex hulls from all contacts are combined to form the grasp wrench space:

$$\mathcal{W} = \text{co}(\mathcal{W}_1, \ldots, \mathcal{W}_k). \tag{2.17}$$

This convex polytope in wrench space represents the total set of net wrenches the grasp can apply to the object, capturing both the magnitude and directionality of the grasp's disturbance resistance. Geometrically, the GWS can be interpreted as a multidimensional volume in wrench space, formed by combining all feasible contact contributions. It is typically visualized as a convex polytope centered around the origin; the larger and more isotropic this space is, the more robust the grasp is against perturbations in multiple directions.

3. **Largest Inscribed Ball (ϵ-metric):** To obtain a single numerical grasp quality score, the ϵ-metric is computed as the radius of the largest ball centered at the origin and fully contained within the GWS[42]:

$$Q_{MIN_W}(\mathcal{W}_1, \ldots, \mathcal{W}_k) = \min_{\mathbf{w} \in \partial \mathcal{W}} \|\mathbf{w}\|. \tag{2.18}$$

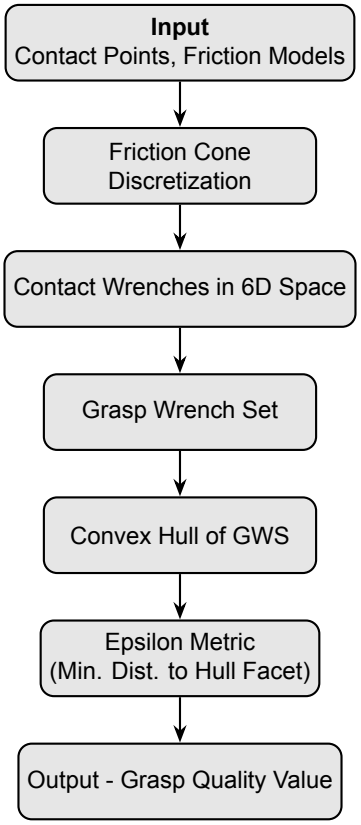

Figure 2.4: Flowchart for computing the ε grasp quality metric

This value corresponds to the maximum disturbance magnitude that can be resisted equally well in all directions. A larger ϵ indicates a more robust and isotropic grasp.

2.4. Chapter summary

This chapter lays the groundwork for semiconductor handling-related gripper design, showing six gripper technologies (mechanical, vacuum, magnetic, electro-adhesive, Bernoulli, and acoustic) and comparing their abilities and limitations for handling silicon MEMS chips. Vacuum-based gripping was selected as the best option to be augmented with passive mechanical stop clamps to protect the sensitive surface features on the MEMS chip. The chapter then establishes complete mathematical frameworks for analysis of grasps, including a friction cone model, wrench space representation, and the ϵ-metric for evaluating the quality of a grasp quantitatively. Together, these theoretical tools allow comparison of grasp types while also meeting handling requirements.

3

Grasp Analysis Methodology and Gripper Design

After looking into the pros and cons of various types of grippers in the previous chapter, the vacuum-based gripper concept is chosen for gripper development. This chapter outlines the GAM for analytical modelling of the gripper designs, in which two important gripper parameters are chosen, i.e., the grasp quality and avoidance of edge chipping through stress analysis. Two grasp designs (three-point grasp and four-point corner grasp) are generated and compared with the industrial state-of-the-art design (referred to as the surface grasp [43]). Figure 3.1 summarizes this GAM workflow and illustrates how each step informed the next in the development of a viable gripper concept.

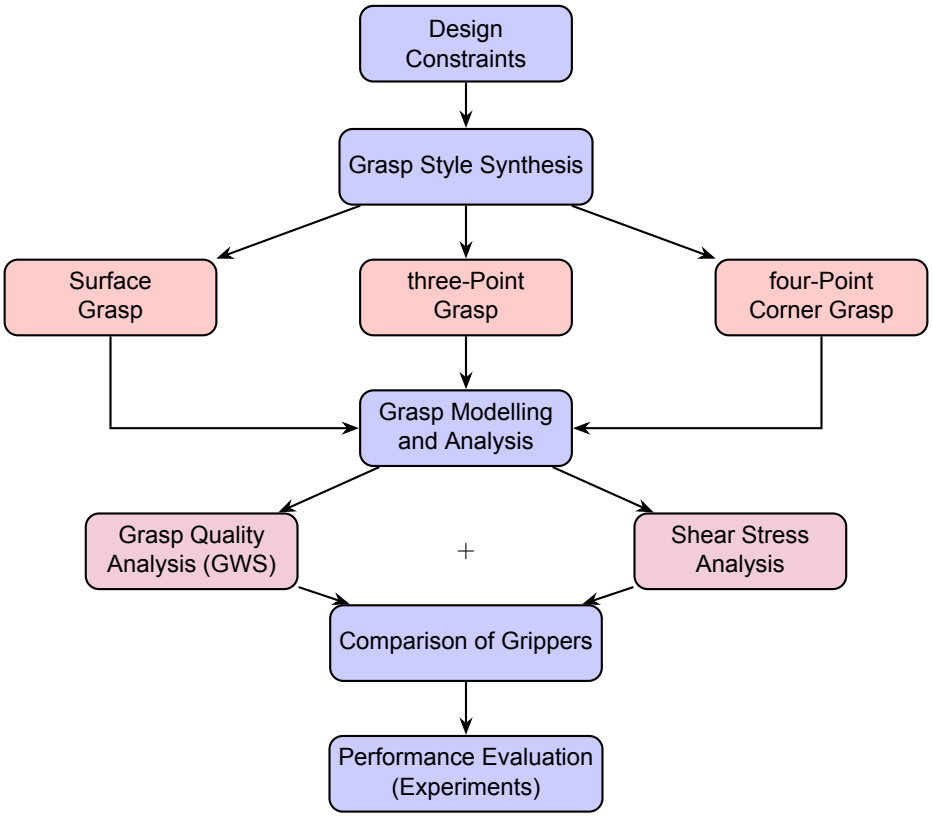

Figure 3.1: Workflow of the Grasp Analysis Methodology (GAM)

3.1. Design constraints and requirements

Before going in to designing grippers, key geometrical constraints and design requirements are established in this section.

3.1.1. Workspace and workpiece definition

The silicon chip, or workpiece, is assumed to lie in the xy plane. It must be constrained in all degrees of freedom except for translation along the z axis, to allow for easy pick and place operation.

Chip safe zones:
In this work, the silicon chips being considered have a total dimension of 5 $mm \times 5$ mm. The sensitive structures are bilayer graphene drums. There are thousands of such drums arranged on the surface of the chip such that they occupy a central area of 4 $mm \times 4$ mm, thus effectively making the central patch a no-go zone (or red zone) for the gripper. This leaves a peripheral patch of 0.5 mm on the chip, which can be considered a safe zone (or green zone) for the gripper.

Wafer workspace:
It is also imperative to expand the workspace to include wafer constraints. This is important as it defines the amount of space available around the chips for approaching and gripping it. For context, the preparation of the chips is briefly described here. The silicon wafer is kept on a UV release tape and then is cut into chips of dimensions 5 $mm \times 5$ mm with the help of a laser. The UV tape ensures that the chips do not move out of position during the laser cutting. Thus, the final wafer has chips which are spaced 0.5 mm apart from each other. This prepared wafer is then exposed to UV light in order to reduce the adhesive forces on the chips and then it is sent for assembly operations.

This effectively means that, in addition to the 0.5 mm peripheral patch on the edge of each chip, there is a 0.5 mm space in between adjacent chips that can be used for grasping the chips.

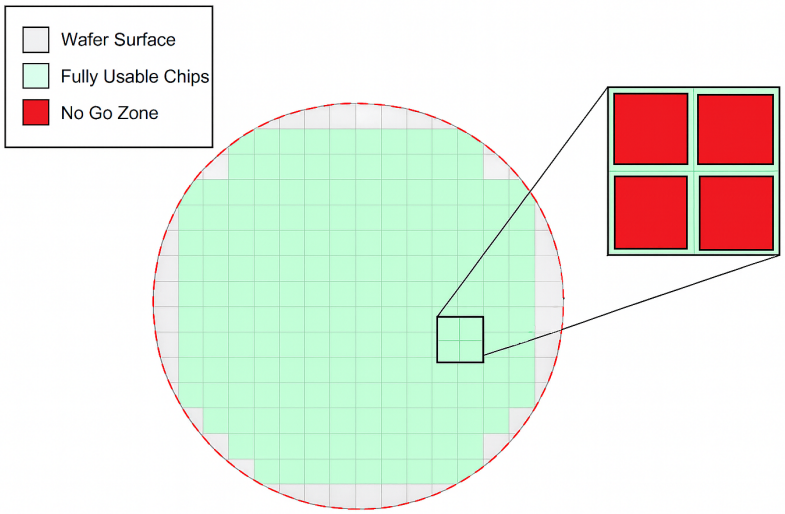

Figure 3.2: Depiction of wafer workspace along with the chip's no go zones

3.1.2. Design requirements

The following design requirements also need to be satisfied by the gripper.

- **Optimal grasp**: Here, an optimal grasp is defined as meeting the all the design constraints and having the highest grasp quality score, given by the ϵ-metric.
- **Minimal edge stress**: Since edge chipping is a common problem in silicon based chips, the designed gripper must have minimum shear force, to effectively reduce shear stresses at the

edges and prevent edge damage.

- **Positional accuracy**: As defined earlier, there is only 0.5 mm of space in between chips on the wafer workspace. This implies that positional accuracy of the gripper after the pick and place operation must fall within these bounds. Also, the diagnostic machine developed by SoundCell B.V. had the placement requirements of $\pm$ 400 microns from the target location as well as rotational placement requirement of 1°.

3.2. Grasp Style Synthesis

With the workspace, workpiece constraints, and safe contact regions defined, the next step is to adapt common industrial grasp strategies into configurations that meet these requirements and can be modelled for quantitative evaluation.

In the current industrial context, manipulation of such silicon chips is typically achieved through two dominant strategies:

- **Surface grasp-** contact is made along a portion of the vertical face of the object (Figure 3.3a).
- **Edge grasp-** the gripper engages with one or more of the chip's peripheral edges (Figure 3.3b).

These grasp styles are prevalent due to their ease of implementation in pick-and-place automation and their ability to provide relatively stable handling in routine operations.

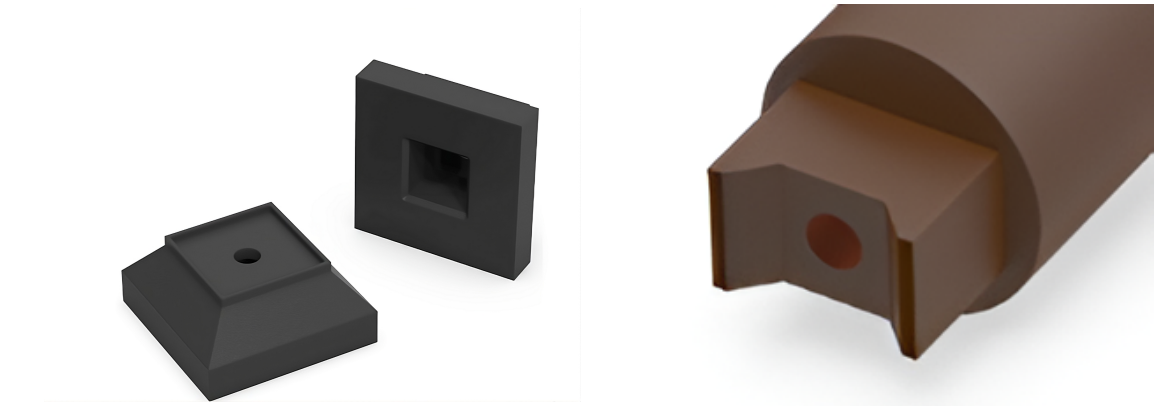

(a) Surface grasp gripper

(b) Side or Edge contact gripper

Figure 3.3: Designs currently being used in the industry for the pick-and-place operations of sensitive chips [43]

Despite their industrial robustness, both configurations are suboptimal when evaluated against the specific design constraints imposed by the design constraints, as outlined in Section 3.1. The Surface grasp, for instance, while effective in constraining translational degrees of freedom (DoFs), fails to provide resistance against rotation about the vertical axis (θ_z). As a result, supplementary guiding mechanisms or increased contact pressure are often necessary to compensate for the underconstrained DoF, which may not be desirable in precision assembly tasks.

The edge grasp, on the other hand, offers the ability to constrain all six DoFs under the assumption of sufficient friction at the contact interfaces. However, the edge regions of the chip are often sensitive to damage. Concentrated loading at these regions may result in micro chipping (as shown in Figure 1.2), localized wear, or long term degradation of part integrity.

Since the edge grasp is more promising, a systematic decomposition is pursued to address its limitations. Specifically, the continuous line contact characteristic of the edge grasp is approximated using a discrete set of point contacts. This modelling approach is supported by prior work in grasp theory, where a line contact can be equivalently represented as two point contacts at its ends, provided local curvature and friction properties are appropriately considered [44]. For planar objects, it is also well established that three non-collinear frictional point contacts are sufficient to achieve force closure in $\mathbb{R}^2$ [45].

The following alternative configurations are therefore examined:

- **Three-point grasp -** derived from decomposing the edge grasp into discrete contacts, resulting in a configuration with three non-collinear point contacts (Figure 3.4b). This serves as an analytically tractable representation for evaluating grasp quality while still relying on contact regions adjacent to the chip edges.
- **Four-point corner grasp -** developed to eliminate edge contact entirely and increase mechanical symmetry (Figure 3.4c). Contact points are positioned at the four corners of the chip, providing zero contact along the edge regions and enhancing passive alignment during placement.

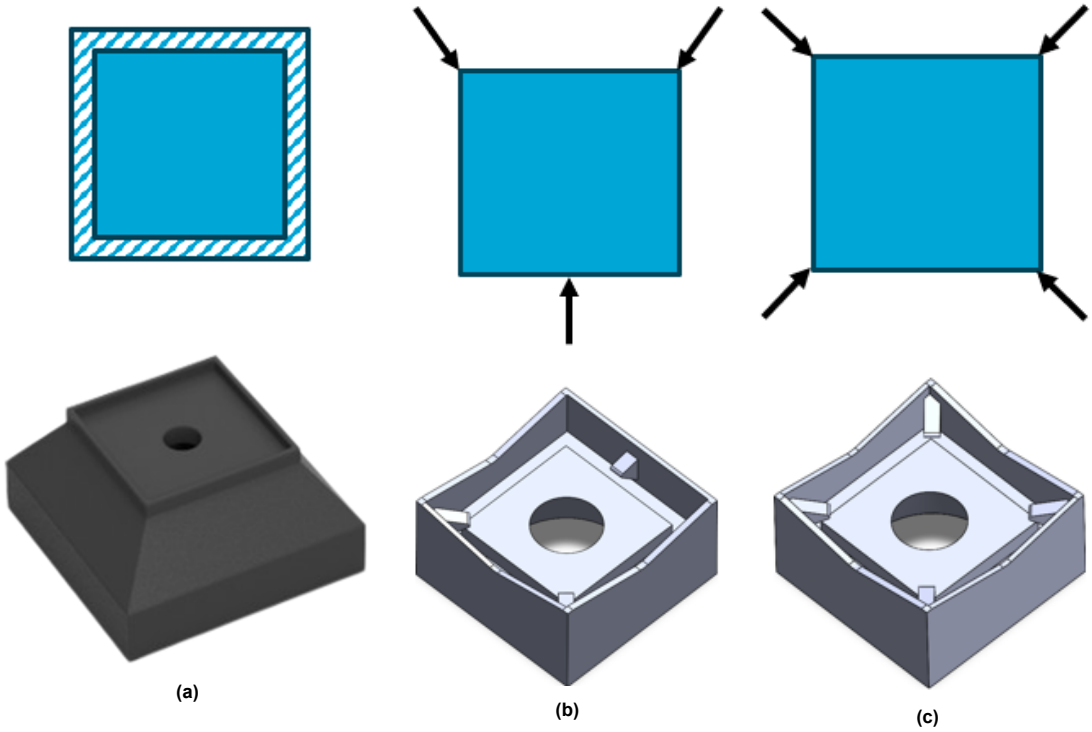

Figure 3.4: Sketches and CAD models of the designs evaluated in the current work (a) surface grasp, (b) three-point grasp and (c) four-point grasp

3.3. Analysis of grasp wrench space

Based on the theoretical formulation in subsection 2.3.3, the three grasp configurations studied in this work are converted into their corresponding wrench space representations. The sum of the forces on the contact locations is bounded to 1N, and the generated friction cones provide the critical forces for the slip condition. The critical forces and torques are written as wrenches at the contact point. These wrenches are then transformed to the equivalent wrenches at the center of mass of the chip.

The results are presented in two stages. First, the convex hull of the wrench space is visualized for each configuration, providing a qualitative view of the range and distribution of feasible wrenches. This is followed by a quantitative comparison using the grasp quality metric, which allows the relative performance of the grasps to be evaluated and the most suitable configuration to be identified.

3.3.1. Wrench space visualization

The wrench space obtained for each grasp is a six-dimensional set. For visualization, two projections are shown with (F_x, F_y, F_z) and (F_z, T_y, T_z) as the coordinate axes, where F_x, F_y, F_z and T_x, T_y, T_z are defined in Figure 3.5.

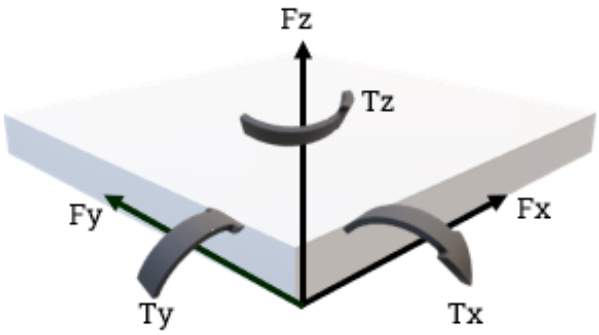

Figure 3.5: Representation of the force and torque directions with respect to the chip

The wrench space representation provides insight into the combinations of forces and torques that will cause the chip to be released from the gripper. A specific combination of forces and torques is represented in the wrench space as a six dimensional vector. If a wrench vector originating at the origin intersects the convex hull, the corresponding combination of forces and torques is sufficient to ungrasp the chip.

In particular, examining the F_z direction illustrates this concept clearly: the minimum force in the F_z direction required to ungrasp the chip corresponds to the magnitude of the wrench vector when it first intersects the convex hull.

Wrench space: Surface grasp

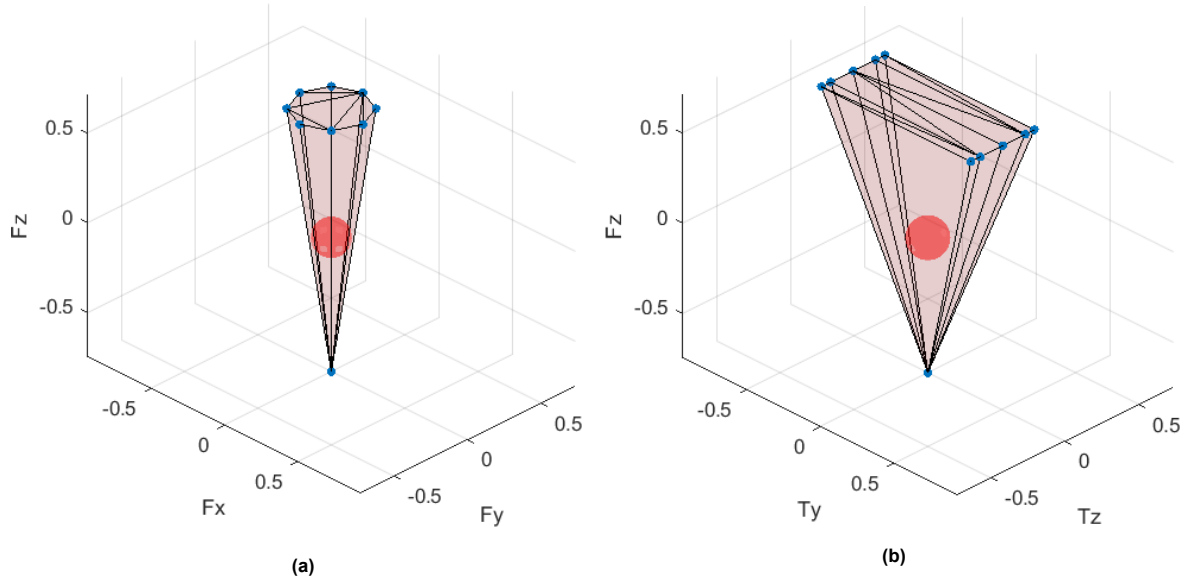

Figure 3.6: 3D wrench space for the surface grasp configuration in two principal subspaces: (a) pure force subspace $F_xF_yF_z$ and (b) force + torque subspace $F_zT_yT_z$. The transparent convex hull represents the feasible wrench set, while the red sphere denotes the largest inscribed ϵ-ball, corresponding to the grasp quality metric.

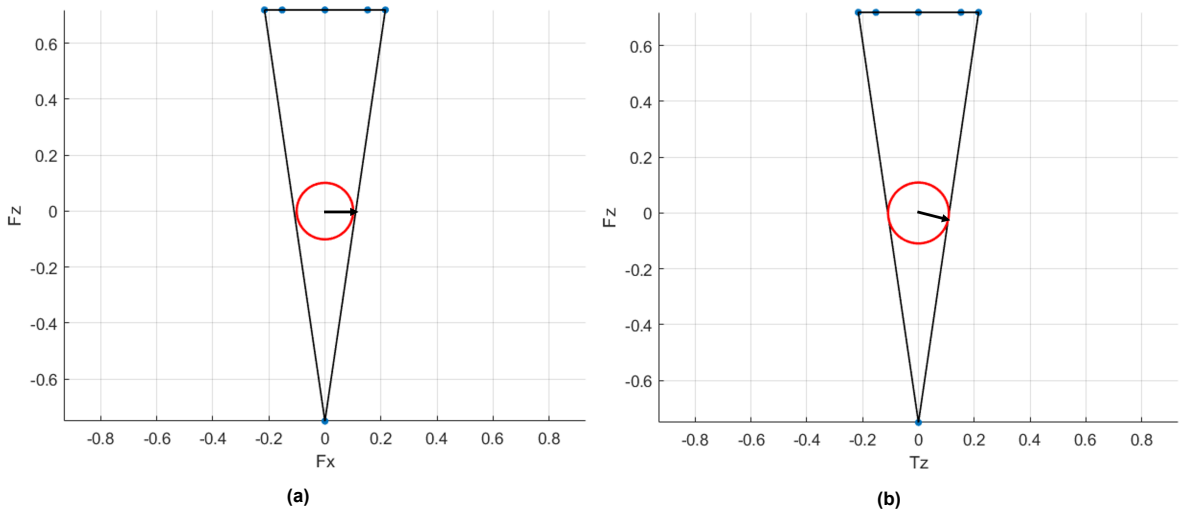

Figure 3.7: 2D projections of the grasp wrench space for the surface grasp configuration in two principal subspaces: (a) pure force subspace $F_xF_yF_z$ projected onto the F_x–F_z plane, and (b) force-torque subspace $F_zT_yT_z$ projected onto the T_z–F_z plane. The black polygon represents the convex hull boundary, while the red circle denotes the largest inscribed ϵ-ball, corresponding to the grasp quality metric, and the black arrow depicts the failure direction of the grasp

The grasp wrench space of the surface grasp provides insight into the directions in which the grasp can effectively resist disturbances and the directions in which it is likely to fail.

The $F_xF_yF_z$ projection shows that the convex hull is relatively wide along the F_z axis, indicating that the grasp can sustain comparatively high vertical forces acting perpendicular to the object plane. In contrast, the convex hull is narrow along the F_x and F_y axes, reflecting a low capacity to resist in plane translational forces. This suggests that while the surface grasp is well-suited to resisting vertical loads, it is vulnerable to horizontal disturbances in the object's plane.

Similarly, the $F_zT_xT_z$ projection reveals limited resistance to torques about the T_z axis. The convex hull is significantly narrower in this direction, consistent with the fact that the surface grasp provides no azimuthal constraint on the object. As a result, even small torsional disturbances about the suction axis could cause object slippage or rotation unless compensated for by external fixtures or active control.

Wrench space: Three-point grasp

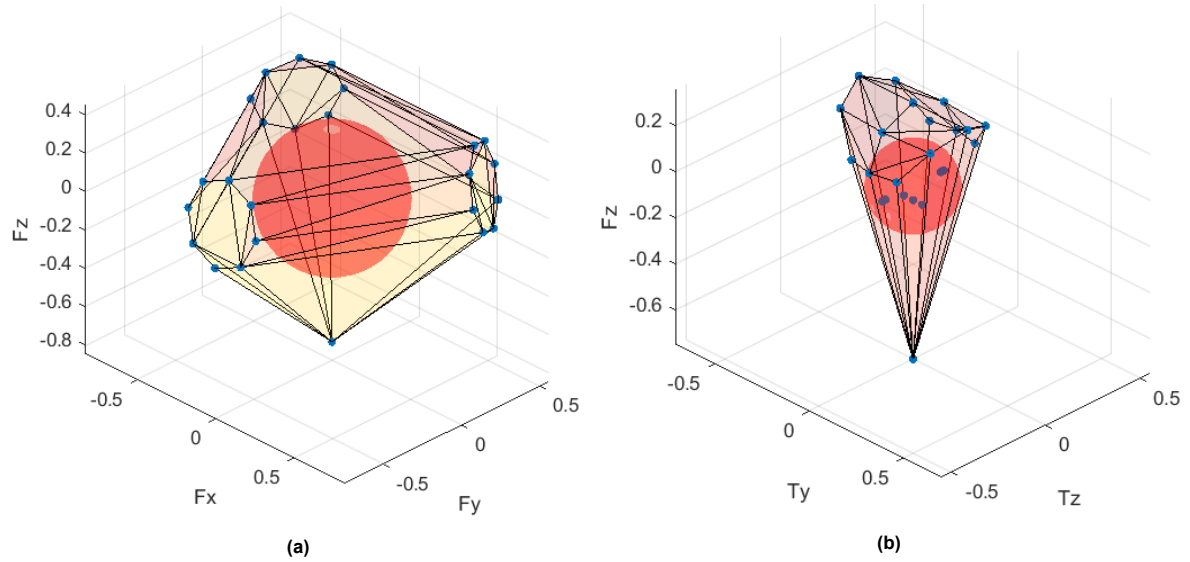

Figure 3.8: 3D grasp wrench space for the three-point grasp configuration in two principal subspaces: (a) pure force subspace $F_xF_yF_z$ and (b) force + torque subspace $F_zT_yT_z$.

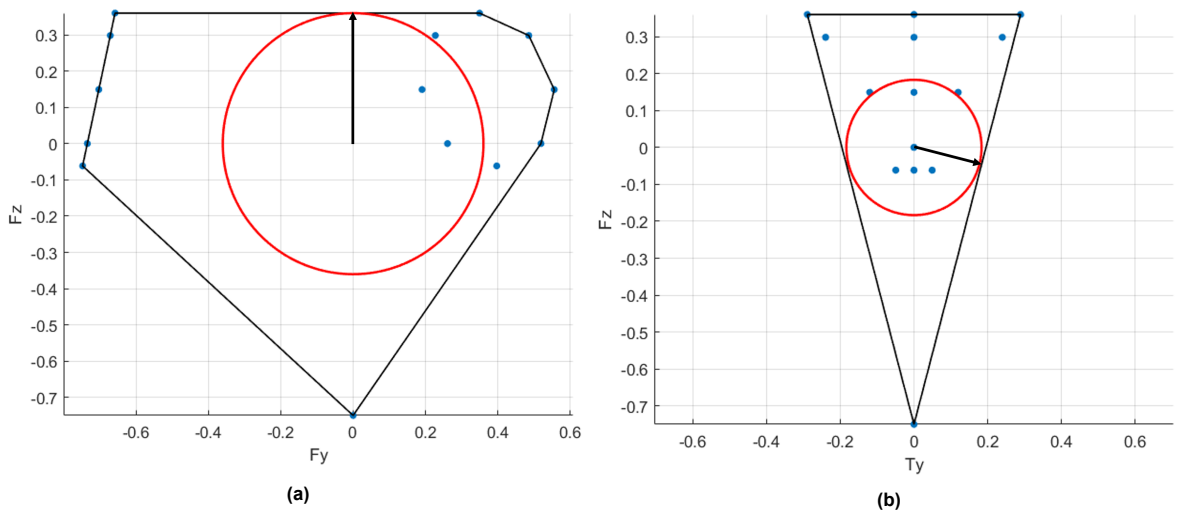

Figure 3.9: 2D projections of the grasp wrench space for the three-p grasp configuration in two principal subspaces: (a) translational subspace $F_yF_yF_z$ projected onto the F_y–F_z plane, and (b) force + torque subspace $F_zT_yT_z$ projected onto the T_y–F_z plane.

Compared to the patch grasp, it offers improved stability in both force and torque spaces, it maintains sufficient wrench coverage across all six degrees of freedom.

The force only wrench space is reasonably isotropic, with a decent ϵ ball radius in Fx, Fy, and Fz. Notably, while the grasp is strongest in Fz, it still offers usable resistance to lateral perturbations; an essential feature for in-plane manipulation.

In the $FzTxTy$ subspaces, the three-point grasp displays a robust ability to resist Tx and Ty, and more interestingly, achieves meaningful resistance in Tz; a weakness in the surface grasp.

This configuration is particularly attractive when minimal contact is desired, or when object geometry limits the number of safe contact zones.

Wrench space: Four-point grasp

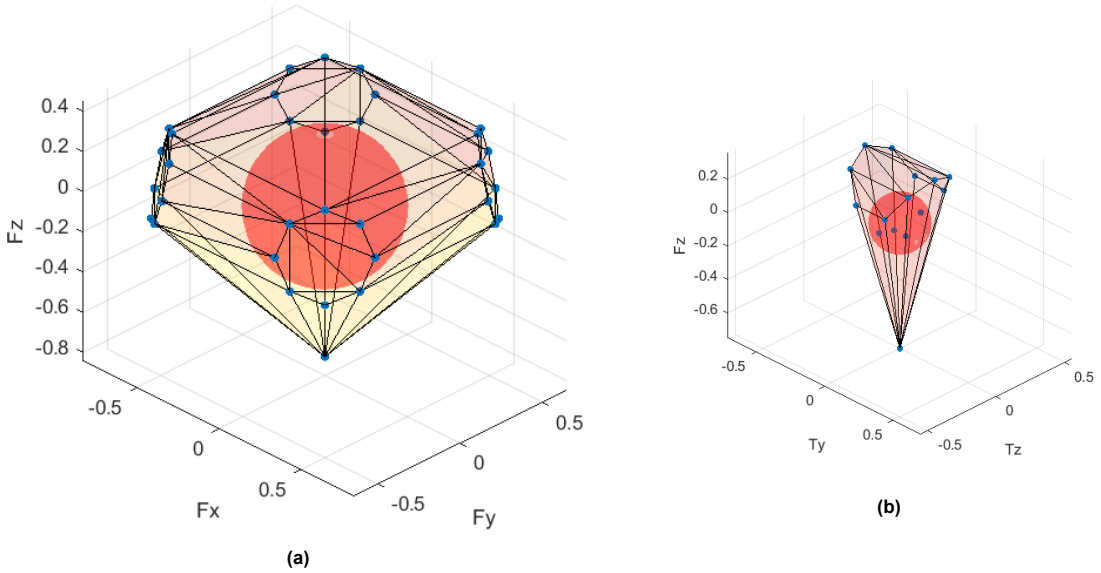

Figure 3.10: 3D grasp wrench space for the four-point grasp configuration in two principal subspaces: (a) pure force subspace $F_xF_yF_z$ and (b) force + torque subspace $F_zT_yT_z$.

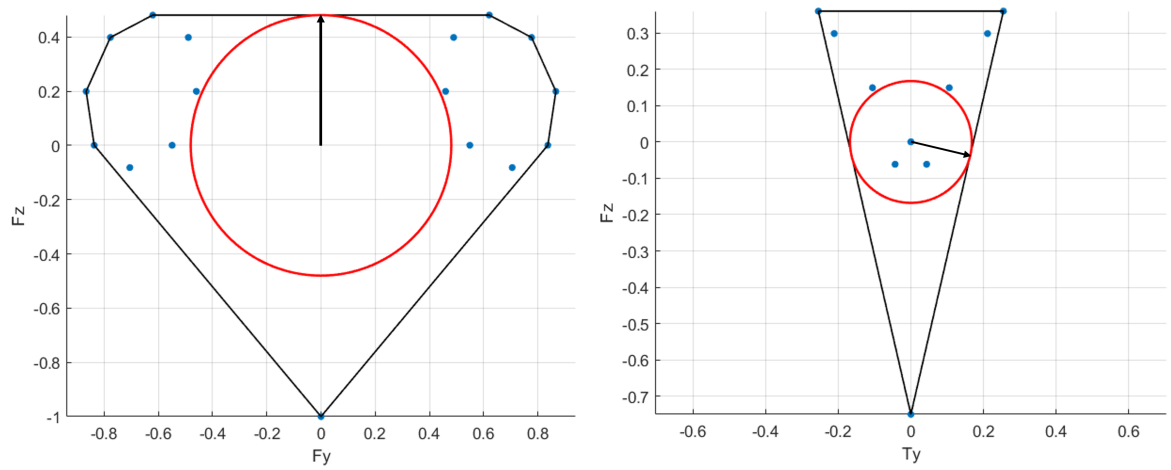

(a) 2D projection

(b) 2D projection

Figure 3.11: 2D projections of the grasp wrench space for the four-p grasp configuration in two principal subspaces: (a) pure force subspace $F_xF_yF_z$ projected onto the F_y–F_z plane, and (b) force + torque subspace $F_zT_yT_z$ projected onto the T_y–F_z plane.

The grasp configuration employing four corner contact points yields a markedly improved wrench space compared to the Surface approach.

This configuration was designed to provide direct point contacts at the object's extremities, thereby maximizing the moment arm available for resisting external torques, which is a weakness of surface grasp grippers.

Analysis of the force-only wrench space shows a broad and symmetric spread in the $F_xF_yF_z$ space. The convex hull captures force resistance in all three translational directions, and the ϵ ball inscribed within the wrench space is significantly larger than that of the perimeter grasp. This indicates a more isotropic and robust grasp, capable of resisting perturbations from arbitrary directions, including planar disturbances.

The improvement arises from the spatial separation of contact points, which introduces the capability to generate counteracting torques; a necessary condition for rotational stability.

This grasp configuration is well-suited to tasks requiring fine manipulation, in-plane translations, and rotational adjustments, such as pick-and-place with orientation control.

A short summary of all the discussions above is briefed in the following Table 3.1

Evaluation Criterion	**Surface Grasp**	**three-Point Grasp**	**four-Point Grasp**
Translational Resistance (F_x, F_y)	Poor; no constraint in-plane	Moderate; slightly anisotropic	High; nearly isotropic resistance
Rotational Resistance (T_x, T_y)	Moderate; from distributed perimeter interaction	Moderate to high; enabled by contact geometry	High; large torque arms due to contact layout
Rotational Resistance (T_z)	Very poor; unconstrained	Moderate; direction-dependent	High; force couples generated by spatial spread

Table 3.1: Qualitative interpretation of grasp wrench-space characteristics and functional capabilities

3.3.2. Comparison based on grasp quality metric

The ϵ-metric values in Table 3.2 report the minimum disturbance magnitude at which the grasp fails (i.e., the radius of the largest origin centered ball contained in the corresponding wrench space projection). Consequently, larger ϵ indicates that a grasp withstands larger disturbances before failure in that subspace, whereas smaller ϵ indicates earlier failure.In our results, the surface grasp shows the lowest metric, followed by the three-point grasp, while the four-point grasp demonstrates the highest metric, indicating the greatest resistance to disturbances.

Grasp Configuration	**ϵ Metric Value (N)**
Surface grasp	0.1089
three-point grasp	0.1151
four-point grasp	0.1648

Table 3.2: ϵ-metric values (failure thresholds) for different subspaces and grasp configurations

Table 3.1 complements these thresholds with a qualitative interpretation of wrench-space morphology (translational and rotational resistance).

Taken together, the threshold values in Table 3.2 and their qualitative interpretation in Table 3.1 indicate that the four-point grasp provides the most robust performance across the considered subspaces. It combines strong translational resistance with the highest rotational threshold in $F_z T_y T_z$ subspace.

3.4. Modeling of shear stresses

A high grasp metric value generally indicates a more stable grasp. However, preventing edge chipping requires additional consideration. Specifically, it is important to ensure that the shear forces exerted by the gripper on the chip do not induce localized stresses that could lead to material chipping at the edges.

To evaluate this risk, a shear stress analysis was conducted using Timoshenko's Classical Plate Theory [46]. The analysis involved applying appropriate boundary conditions corresponding to each grasp configuration, which is summarised in Table 3.3. A higher shear stress implies an increased likelihood of edge chipping. This highlights the critical role of minimizing stress concentrations during gripping.

For the analysis, a uniform distributed loading is assumed on an isotropic material with a Poisson's ratio of 0.3. Timoshenko's Classical Plate Theory [46] and the work of [47] were used for the shear stress calculations, along with the standard assumptions of classical plate theory.

For a surface patch grasp, simply supported boundary conditions were considered. In the case of the three-point grasp, the boundary conditions correspond to a plate clamped along two edges, with the remaining edges free. This configuration arises from decomposing the three-point gripper from the edge gripping setup, allowing the analysis to be simplified to this equivalent plate model. For a four-point corner grasp, the boundary conditions are a plate simply supported at the corner points.

While the choice of a point contact gripper may seem counterintuitive due to the potential for stress concentrations at the corners, the final stress values obtained from the analysis indicate that, even with concentration factors considered, the stresses remain well below the yield stress of silicon. The calculated stress values, which are in the range of kPa, suggest that the gripper design is safe with respect to material failure.

3.5. Analysis of shear force

For a uniformly distributed transverse load q_0, the maximum transverse shear force per unit length $Q_{x,max}$ for each configuration is computed using classical plate theory solutions is presented in Table 3.4.

Grasp Configuration	Plate Boundary Conditions	Illustration
Surface grasp	$w = 0, \quad \frac{\partial w}{\partial x} = 0$ at $x = \pm a$ $M_y = 0, \quad V_y = 0$ at $y = \pm b$	
Three-point grasp	$w = 0, \quad \theta_x = 0$ at $x = \pm a$ $M_y = 0, \quad V_y = 0$ at $y = \pm b$	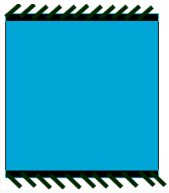
Four-point corner grasp	$w = 0$ at corners $M_x = 0, \quad V_x = 0$ at $x = 0, a$ $M_y = 0, \quad V_y = 0$ at $y = 0, b$	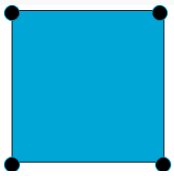

Table 3.3: Plate boundary conditions for different grasp configurations

Grasp Configuration	$Q_{y,\max}(\beta q a)$ (N/mm)
Surface grasp	0.0506
Three point grasp	0.3462
Four point grasp	0.0301

Table 3.4: Maximum transverse shear forces ($Q_{x,\max}$) for different grasp configurations under equivalent loading conditions

Comparing the stress concentration factors for the shear stresses of the three grasp types, it is seen that the four-point grasp has the lowest stress concentration factors, and thus the lowest chance of suffering from edge chipping.

3.6. Chapter summary

This chapter presented a detailed evaluation of three candidate gripper configurations: surface grasp, three-point grasp, and four-point corner grasp by using grasp wrench space (GWS) analysis and shear stress assessment. The GWS visualisation provided insight into the force-torque subspaces where each grasp is most vulnerable, while the ϵ-metric quantified the disturbance magnitude required to cause grasp failure in each subspace. The shear stress analysis complemented these results by estimating the maximum transverse shear forces experienced under equivalent loading conditions.

The combined results indicate that the surface grasp offers limited resistance to in-plane forces and torques, the three-point grasp provides improved but anisotropic resistance (i.e. the gripper's resistance is stronger in some directions and weaker in others.), and the four-point corner grasp delivers the highest and most isotropic resistance (i.e. the gripper can resist forces and torques equally well in all directions of the subspace being evaluated.) across all evaluated subspaces. Based on these findings, the four-point corner grasp was identified as the most suitable configuration for the target application.

4

Experimental Validation and Discussion

This chapter presents the experimental validation and benchmarking of the gripper designs developed through grasp wrench space (GWS) analysis. Three sets of experiments were conducted to evaluate different aspects of gripper performance. First, pull tests were performed to validate the GWS predictions by assessing each gripper's resistance to out-of-plane loading. Second, placement tests were conducted to benchmark the practical performance of the grippers in accurately placing chips onto a target surface. Finally, a graphene membrane integrity test was carried out to determine whether the graphene structures on the chip substrate remain undamaged under vacuum-based gripping. Together, these experiments provide a comprehensive assessment of the mechanical stability, functional performance, and material safety of the proposed gripper designs.

4.1. Experimental evaluation of grasp modeling

To validate the predictions from the grasp wrench space (GWS) analysis, experimental pull tests were conducted to assess each gripper's resistance to out of plane loading along the Z-axis; the axis relevant to the suction-based pick-and-place operation. Two grasp configurations were considered in this study: (i) the three-point grasp as shown in Figure 4.1a, and (ii) the four-point grasp as shown in Figure 4.1b.

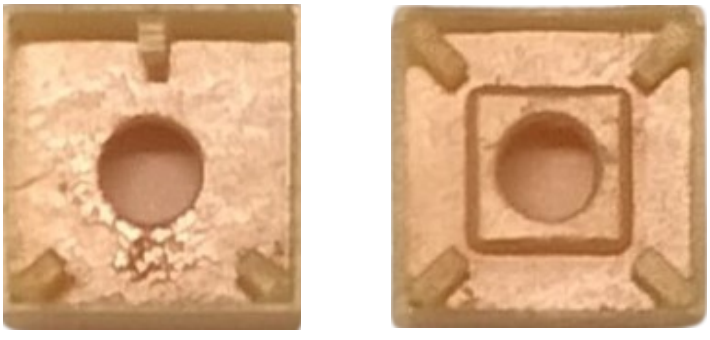

(a) (b)

Figure 4.1: 3D printed models of the developed gripper designs

The surface grasp was excluded, as the failure directions identified through GWS analysis were primarily in plane specifically, translations along X and Y and rotation about the Z-axis. Given the distributed nature of its contact and the absence of lateral constraint, the configuration's inability to resist in-plane disturbances was straightforward to infer from the analytical results. Therefore, out-of-plane torque testing was not carried out for this grasp, unlike the other configurations.

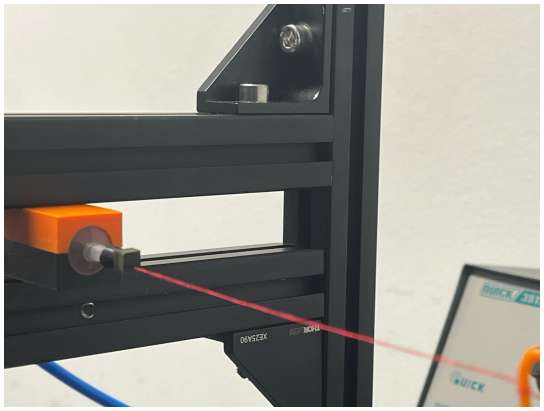

Figure 4.2: Setup for the out of plane torque test

To further interpret the grasp wrench space (GWS) developed using the theory from Sections 3.4 and 3.5, the ϵ metric was computed within the $FzTxTy$ subspace for the two tested configurations: (i) the three-point grasp, and (ii) the four-point grasp. This subspace was selected as it represents the dominant directions of out of plane loading; specifically, the vertical lifting force and the torques that cause chip tilting during manipulation. The resulting ϵ values reflect the relative ability of each configuration to generate wrenches in this subspace, and therefore to resist such perturbations.

To validate the metric calculated by analysing the GWS, pull tests were performed by applying a horizontal force at the right side of the object (at a distance of 2.5mm from the object's centre of mass), while suction was applied on the object's left side. Although the applied force is horizontal, this asymmetric loading induces both a vertical force (Fz) and torques about the X and Y axes (Tx, Ty), making it representative of disturbances in the $FzTxTy$ subspace of the grasp wrench space. The resulting force displacement curves reveal how each grasp configuration responds to such combined loading. The behavior of the three- and four-point grippers under this condition is presented in the following figures.

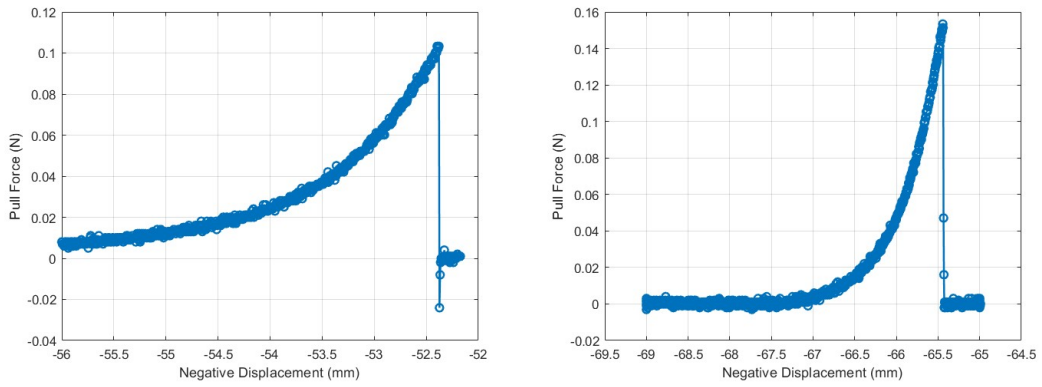

(a) Pull test for three-point gripper

(b) Pull test for four-point gripper

Figure 4.3: Out of plane torque test results of the gripper designs

The force-displacement curve for the three-point gripper exhibits a gradual increase in pull force followed by a sharp drop, indicating the onset of slippage or loss of contact stability. The peak pull force achieved was approximately 0.11 N (or 0.275 Nmm of out of plane torque), beyond which the grasp could no longer sustain the vertical load. The lack of moment balancing in the configuration contributes to lower resistance against tilting and rotation, corroborating the grasp wrench space (GWS) prediction of limited out of plane robustness.

The four-point gripper shows a more pronounced and steeper force build-up, peaking at approximately

0.15 N (or 0.375Nmm of out of plane torque) before the object decouples. Compared to the three-point configuration, the four-point grasp achieves a higher maximum pull force, indicating improved resistance to vertical disturbances. This confirms the higher grasp quality and wrench coverage predicted analytically in the $FzTxTy$ subspace.

Grasp Configuration	**ϵ Metric Value (N)**	**Experimental Values(N)**	**% Difference**
three-point grasp	0.1151	0.11	4.63(-)
four-point corner grasp	0.1677	0.15	10.18(-)

Table 4.1: Comparison of ϵ metric values in the $FzTxTy$ subspace for three-point and four-point grasps

The observed deviations of approximately 4% and 10% between the predicted and experimental ϵ values can be attributed to a combination of geometric, experimental, and material factors:

1. The experimental loading was performed true to the intended setup, aiming to apply torque about the T_y axis. However, the ϵ-direction from the grasp wrench space analysis was found to be slightly inclined rather than perfectly aligned with T_y. This inclination means that the metric value corresponds to a direction that can be resolved into a T_y component along with a small orthogonal component. Resolving the inclined ϵ-direction into its T_y component would yield a closer match to the experimental measurement.
2. During the experimental setup, the applied load was intended to generate a pure torque. However, even a small angular misalignment in the loading tool can result in a portion of the applied force projecting onto the F_x, F_y, or F_z directions, thus altering the measured resistance.
3. The gripper designs had some wall warpage which might have caused an unwanted contact with the object. This unwanted contact, combined with possible differences in surface roughness, may have increased the frictional interaction with the gripper walls, leading to slightly higher resistance than predicted by the model. In order to eliminate this problem, the gripper walls were given slots in it which prevents any unwanted contact with the object's side faces.

4.2. Placement tests

To evaluate the placement accuracy of each gripper, chips were released from a height of 0.5 mm above the target surface. This setup simulates the realistic scenario where chips are placed onto a substrate (e.g. adhesive layer), and direct gripper to substrate contact must be avoided to prevent contamination or interference. RMS errors in translation and rotation were recorded from high-resolution imaging of the final chip positions.

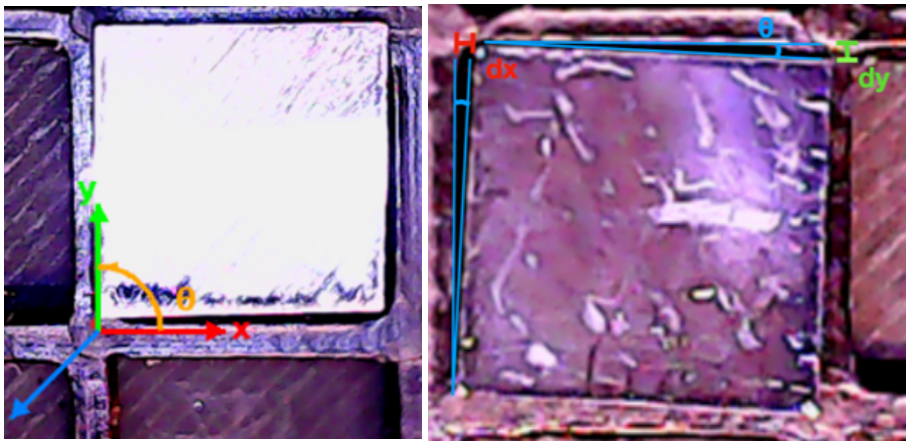

(a) Initial orientation **(b)** Final orientation

Figure 4.4: Translational placement accuracy performance of the gripper designs

4.2.1. Translational placement accuracy

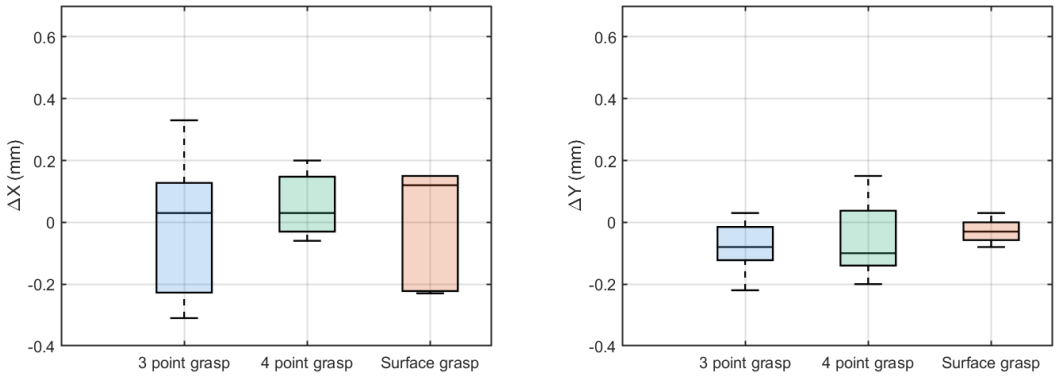

(a) Distribution of position placement error in the x-direction

(b) Distribution of position placement error in the y-direction

Figure 4.5: Translational placement accuracy distribution of the gripper designs. The number of experiments are, for 3 point grasp, N = 10, for 4 point grasp, N = 10 , for surface grasp, N = 10

The box plot provides a detailed view of the distribution of X and Y directional errors for each grasp configuration.

For X direction, the three-point grasp displayed a large spread from approximately $0.31mm$ to $+0.32mm$ with a median close to 0, indicating high variability. The four-point grasp exhibited a narrower range from approximately $0.05mm$ to $+0.20mm$ with a median close to zero, demonstrating consistent performance. The Surface grasp had a moderate range from approximately $0.23mm$ to $+0.18mm$ with a median near $+0.15mm$, reflecting intermediate stability.

For Y direction, the three-point grasp displayed a range from approximately $0.19mm$ to $+0.03mm$ with a median near $0.08mm$. The 4 point grasp exhibited a range from approximately $0.20mm$ to $+0.16mm$ with a median near $0.06mm$. The Surface grasp had the narrowest range from approximately –$0.07mm$ to $+0.04mm$ with a median near $0.02mm$

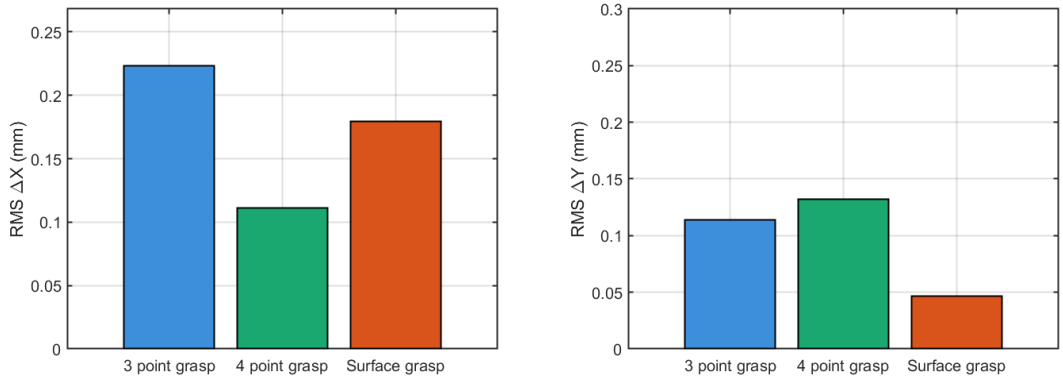

(a) Position placement error in the x-direction

(b) Position placement error in the y-direction

Figure 4.6: Translational placement accuracy performance of the gripper designs

The three-point grasp showed the highest RMS error of approximately $0.223mm$, indicating lower accuracy in the X-direction and greater variability across trials. The four-point grasp recorded the lowest RMS error of approximately $0.111mm$. The Surface grasp achieved an RMS error of approximately $0.180mm$, performing better than the three-point grasp but not as well as the four-point grasp.

The four-point grasp showed the highest RMS error of approximately $0.130mm$, indicating slightly lower

accuracy in the Y-direction compared to the other grasps. The three-point grasp recorded an RMS error of approximately $0.115mm$. The Surface grasp achieved the lowest RMS error of approximately $0.046mm$. The three-point grasp showed the highest RMS error of approximately $0.223mm$, indicating lower accuracy in the X-direction and greater variability across trials. The four-point grasp recorded the lowest RMS error of approximately $0.111mm$. The Surface grasp achieved an RMS error of approximately $0.180mm$, performing better than the three- point grasp but not as well as the four-point grasp.

4.2.2. Rotational placement accuracy

The rotational placement accuracy of three grasp configurations, three-point grasp, four-point grasp, and Surface grasp, were evaluated. The results are presented as both the Root Mean Square (RMS) error in a bar graph and the full error distribution in a box plot.

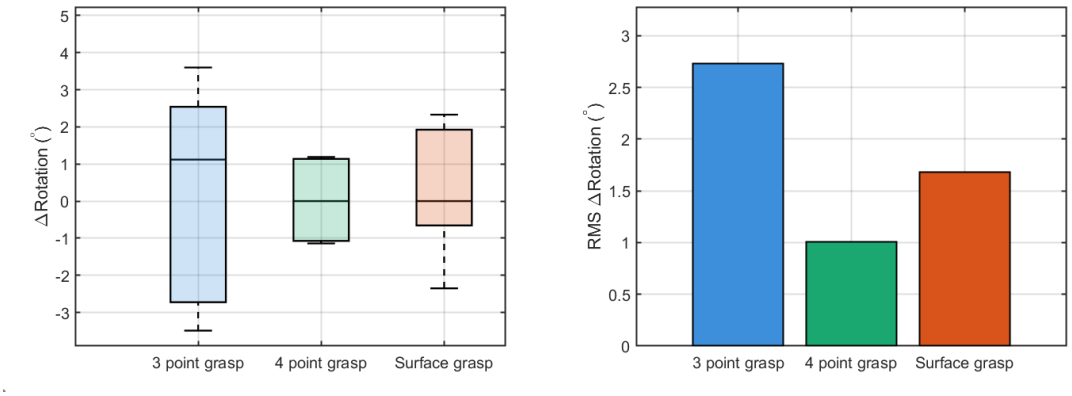

(a) Distribution of rotational placement error

(b) Rotational placement error

Figure 4.7: Rotational placement accuracy performance of the gripper designs

The three-point grasp showed the highest RMS error of approximately 2.73°, indicating lower rotational accuracy and greater variability across trials. The four-point grasp recorded the lowest RMS error of approximately 1.01°, reflecting a high degree of control and repeatability. The Surface grasp achieved an RMS error of approximately 1.69° performing better than the three-point grasp but not as well as the four-point grasp. These values highlight that increasing the number of contact points from three to four significantly improves rotational stability during placement.

The box plot provides a detailed view of the distribution of rotational errors for each grasp configuration. The three-point grasp displayed a large spread from approximately -3.3° to +3.6° with a median slightly above +1°, indicating high variability and a tendency towards positive rotation. The four-point grasp exhibited a narrow range from approximately -1.1° to +1.2° with a median close to zero, demonstrating consistent performance and minimal bias in either rotational direction. The Surface grasp had a moderate range from approximately -1.8° to +2.3° with a median near zero, reflecting intermediate stability and accuracy.

Overall, the four-point grasp demonstrated the highest rotational accuracy, achieving both low error magnitude and low variability. The Surface grasp performed moderately well, while the three-point grasp exhibited substantial deviations and instability.

The surface grasp offered good translational stability in the y-direction but lacked effective rotational constraint. The three-point grip suffered from high rotational error due to limited torque resistance. The four-point corner grasp showed the most balanced performance.

4.3. Graphene membrane integrity test

To examine the compatibility of vacuum-based handling with the fragile bilayer graphene membranes, a membrane integrity test was performed. The goal was to determine whether suspended graphene

drums remain intact after brief exposure to vacuum suction, as used in the gripper's pick-up action. Each chip was inspected under a microscope before and after vacuum application, with a white light with blue filter for enhanced visibility of the suspended regions. The vacuum was applied for an estimated duration of 2 to 3 seconds to simulate typical grasping conditions. The four-point corner gripper is used for this purpose.

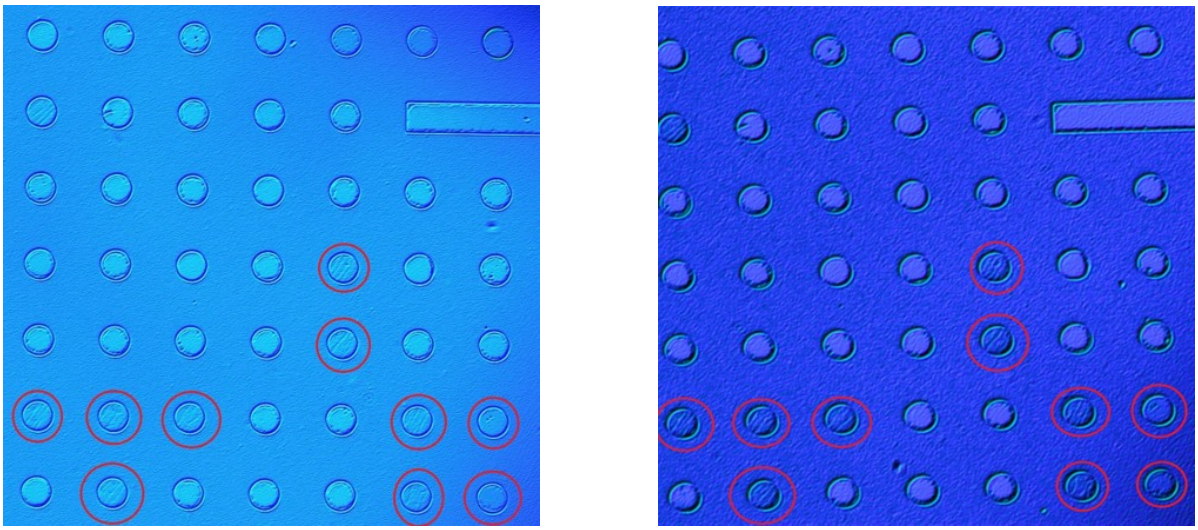

(a) Suspended drums before vacuum action

(b) Same drums after vacuum action

Figure 4.8: Graphene membrane integrity test: comparison before and after vacuum action

The post-grasp inspection images were compared against the pre-grasp state to evaluate any damage or collapse of the suspended regions. The graphene drums, identified and circled in red in both image sets, served as reference points to track membrane condition. After illumination of the chip using white light with blue filter, suspended drums appeared distinctly darker than collapsed or supported regions, enabling clear visual identification [48]. Following vacuum exposure, all marked drums were found to retain their suspended structure. These observations confirm that the bilayer membranes preserved their structural integrity under the applied vacuum conditions.

4.4. Chapter summary

After identifying the four-point gripper as the optimal design based on grasp wrench space (GWS) analysis, a series of experimental evaluations were conducted, including pull tests, placement accuracy tests, and graphene integrity assessments. The placement tests demonstrated that the four-point gripper consistently achieved stable and precise positioning of the chips. Pull test results showed good agreement with the GWS predictions, thereby validating the metric as a reliable measure of grasp robustness. Graphene integrity tests confirmed that all three gripper designs were capable of manipulating the chips without damaging the sensitive graphene surface. However, the four-point gripper offered the best overall performance across both the analytical and experimental evaluations, making it a suitable choice for the intended application.

5

Conclusion

This work explored the design, evaluation, and validation of vacuum-based gripper configurations for the precise handling of chips with suspended bilayer graphene membranes. Recognizing the extreme fragility of such membranes, the study emphasized both mechanical performance and structural compatibility with the object surface. A novel gripper design and analysis technique, i.e. the Grasp Analysis Methodology (GAM) workflow is also simultaneously developed to realize thesis objectives effectively.

Three grasp configurations were examined: a surface grasp (commonly used in industry), a three-point grasp (derived through decomposition of an industrial edge gripper), and a four-point corner grasp (proposed as an alternative for improved stability). Each configuration was modeled using boundary conditions representative of its physical contact pattern.

The Grasp Wrench Space (GWS) analysis was first employed to evaluate the theoretical ability of each grasp to resist external forces and torques, particularly in out-of-plane directions. This provided a comparative understanding of the stability characteristics of the grasps, with the four-point configuration exhibiting the highest ϵ metric value of $0.1677N$, indicating superior predicted resistance to ungrasping forces. To complement the GWS-based findings, a force analysis was then performed using classical plate theory, which estimated the transverse shear forces induced on the chip under each grasp configuration. This allowed further insight into how mechanical loads are distributed depending on the grasp type; with the three-point grasp, for example, producing higher localized shear due to its constraint pattern.

Theoretical predictions were validated through a set of targeted experiments, including pull tests for grasp strength and placement tests for positioning accuracy, with results indicating that the four-point gripper performing better than the other designs.

Graphene membrane integrity tests were performed to assess the survivability of the suspended structures under vacuum. Microscope based inspections before and after grasping confirmed that the bilayer membranes remained intact, indicating compatibility of the vacuum based grasping approach.

Overall, this work demonstrates how a combined approach; linking grasp wrench modeling, mechanical force estimation, and experimental validation can guide the design of grippers for delicate, micro-scale objects. The methodology developed here provides a transferable framework for assessing grasp strategies in semiconductor applications, where both stability and surface sensitivity are critical.

Future Work

While this work focused on rigid gripper configurations and vacuum based pick up of fragile graphene on chip systems, the methodology developed here presents opportunities for broader application and extension.

One direction for future work is the design of specialized grippers tailored to objects with specific geometries, where the integration of Grasp Wrench Space analysis and classical force modeling can guide

contact placement and suction pad design. This is particularly relevant for automated pick and place systems, where precise handling of delicate or non standard components is essential.

Additionally, the framework can be extended to evaluate the grasp quality of compliant grippers that involve multiple points of soft contact. In such cases, where traditional rigid body assumptions may not hold, the ability to approximate or experimentally validate the distribution of contact forces becomes increasingly important. Applying the current approach to soft or adaptive gripping systems could provide insight into how compliance affects grasp stability and object safety, especially for fragile or deformable components.

References

[1] Han Zhang et al. “A Review of Symmetric Silicon MEMS Gyroscope Mode-Matching Technologies”. In: *Micromachines* 13.8 (2022), p. 1255. doi: 10.3390/mi13081255. url: https://doi.org/10.3390/mi13081255.

[2] Chunmei Li et al. “A Review of Wafer-Level Packaging Technology for SAW and BAW Filters”. In: *Micromachines* 16.3 (2023), p. 320. doi: 10.3390/mi16030320. url: https://doi.org/10.3390/mi16030320.

[3] Wei-Sheng Lei, Ajay Kumar, and Rao Yalamanchili. “Die Singulation Technologies for Advanced Packaging: A Critical Review”. In: *Journal of Vacuum Science & Technology B* 30.4 (2012), p. 040801. doi: 10.1116/1.3700230. url: https://doi.org/10.1116/1.3700230.

[4] Nitin Sudani, Krishnan Venkatakrishnan, and Bo Tan. “Laser Singulation of Thin Wafer: Die Strength and Surface Roughness Analysis of 80 µm Silicon Dice”. In: *Optics & Laser Engineering* 47.7–8 (2009), pp. 850–854. doi: 10.1016/j.optlaseng.2009.01.009. url: https://doi.org/10.1016/j.optlaseng.2009.01.009.

[5] Shou-Yao Luo and Zhi-Wei Wang. “Studies of Chipping Mechanisms for Dicing Silicon Wafers”. In: *International Journal of Advanced Manufacturing Technology* 35 (2008), pp. 1206–1218. doi: 10.1007/s00170-006-0800-3. url: https://doi.org/10.1007/s00170-006-0800-3.

[6] Keunhoi Kim et al. “Plasma Dicing Before Grinding for Highly Reliable Singulation of Large, Low-Profile Dies”. In: *Micro and Nano Systems Letters* 11 (2023), p. 16. doi: 10.1186/s40486-023-00183-w. url: https://doi.org/10.1186/s40486-023-00183-w.

[7] SoundCell BV. *Technology — SoundCell*. Accessed 6 July 2025. 2025. url: https://soundcell.nl/technology/ (visited on 07/06/2025).

[8] Irek E. Rosłoń et al. “Probing nanomotion of single bacteria with graphene drums”. In: *Nature Nanotechnology* 17 (2022), pp. 637–642. doi: 10.1038/s41565-022-01111-6.

[9] G. Dini, G. Fantoni, and F. Failli. “Grasping leather plies by Bernoulli grippers”. In: *CIRP Annals* 58.1 (2009), pp. 21–24. issn: 0007-8506. doi: https://doi.org/10.1016/j.cirp.2009.03.076. url: https://www.sciencedirect.com/science/article/pii/S0007850609000298.

[10] J. S. Ervin, N. V. Suryanarayana, and Hon Chai Ng. “Radial, Turbulent Flow of a Fluid Between Two Coaxial Disks”. In: *Journal of Fluids Engineering* 111.4 (Dec. 1989), pp. 378–383. issn: 0098-2202. doi: 10.1115/1.3243656. eprint: https://asmedigitalcollection.asme.org/fluidsengineering/article-pdf/111/4/378/5900073/378_1.pdf. url: https://doi.org/10.1115/1.3243656.

[11] Marco A. B. Andrade et al. “Contactless pick-and-place of millimetric objects using inverted near-field acoustic levitation”. In: *Applied Physics Letters* 116.5 (Feb. 2020), p. 054104. issn: 0003-6951. doi: 10.1063/1.5138598. eprint: https://pubs.aip.org/aip/apl/article-pdf/doi/10.1063/1.5138598/14531997/054104_1_online.pdf. url: https://doi.org/10.1063/1.5138598.

[12] Marc Röthlisberger et al. “Contactless Picking of Objects Using an Acoustic Gripper”. In: *Actuators* 10.4 (2021). issn: 2076-0825. url: https://www.mdpi.com/2076-0825/10/4/70.

[13] Martin Phelan and Cosme Furlong. “Characterization of a MEMS Electrostatic Microgripper for Micromanipulation and Sensing”. In: *Micro and Nanomechanics, Volume 5*. 2018, pp. 65–72. doi: 10.1007/978-3-319-63405-0_11. url: https://doi.org/10.1007/978-3-319-63405-0_11.

[14] Maxence Leveziel et al. “MiGriBot: A miniature parallel robot with integrated gripping for high-throughput micromanipulation”. In: *Science Robotics* 7.69 (2022), eabn4292. doi: 10.1126/scirobotics.abn4292. eprint: https://www.science.org/doi/pdf/10.1126/scirobotics.abn4292. url: https://www.science.org/doi/abs/10.1126/scirobotics.abn4292.

[15] Jeffrey Krahn, Francesco Fabbro, and Carlo Menon. “A Soft-Touch Gripper for Grasping Delicate Objects”. In: *IEEE/ASME Transactions on Mechatronics* PP (Feb. 2017), pp. 1–1. doi: 10.1109/TMECH.2017.2663322.

[16] Chih-Hsing Liu et al. “Optimal Design of a Motor-Driven Three-Finger Soft Robotic Gripper”. In: *IEEE/ASME Transactions on Mechatronics* 25.4 (2020), pp. 1830–1840. doi: 10.1109/TMECH.2020.2997743.

[17] Sara Marullo et al. “The Mag-Gripper: A Soft-Rigid Gripper Augmented With an Electromagnet to Precisely Handle Clothes”. In: *IEEE Robotics and Automation Letters* 5.4 (2020), pp. 6591–6598. doi: 10.1109/LRA.2020.3015719.

[18] Sònia Donaire et al. “A Versatile Gripper for Cloth Manipulation”. In: *IEEE Robotics and Automation Letters* 5.4 (2020), pp. 6520–6527. doi: 10.1109/LRA.2020.3015172.

[19] M. Bonilla et al. “Grasping with Soft Hands”. In: *2014 IEEE-RAS International Conference on Humanoid Robots*. 2014, pp. 581–587. doi: 10.1109/HUMANOIDS.2014.7041421.

[20] Jie Xu et al. “Selecting and Designing Grippers for an Assembly Task in a Structured Approach”. In: *arXiv preprint arXiv:2003.04087* (2020).

[21] H Llewellyn-Evans, CA Griffiths, and A Fahmy. “Microgripper design and evaluation for automated µ-wire assembly”. In: *Microsystem Technologies* 25.8 (2019), pp. 3081–3094.

[22] Seung Baek and Dong Oh Kim. “Predictive Process Adjustment by Detecting System Status of Vacuum Gripper in Real Time during Pick-Up Operations”. In: *Processes* 9.4 (2021), p. 634.

[23] Yongjoon Yoo et al. “Compliant suction gripper with seamless deployment and retraction for robust picking against depth and tilt errors”. In: *arXiv preprint arXiv:2211.16090* (2022).

[24] Seongjun Song et al. “Suction-based soft robotic gripping of rough and irregular parts”. In: *arXiv preprint arXiv:2009.08156* (2020).

[25] Woochan Lee et al. “Vertical magnetic-field-assisted self-assembly of microchips”. In: *Microsystems & Nanoengineering* 5.1 (2019), pp. 1–8.

[26] MIT News. *“Electroadhesive” stamp picks up and puts down microscopic LED chiplets*. Online. Available at: https://news.mit.edu/2019/electroadhesive-led-pick-place-0812. 2019.

[27] Bo N. J. Persson and Jianglong Guo. *Electroadhesion for soft adhesive pads and robotics: theory and numerical results*. 2019.

[28] Ryo K. Kanno et al. *Hybrid Soft Electrostatic Metamaterial Gripper for Multi-surface, Multi-object Adaptation*. 2024.

[29] Jianglong Guo, Bo N. J. Persson, and Metin Sitti. “Electroadhesion Technologies for Robotics: A Comprehensive Review”. In: *IEEE Transactions on Robotics* 36.2 (2020), pp. 338–354.

[30] T. Ali, L. Zhang, and Y. Chen. “Optimization of Outer Diameter Bernoulli Gripper with Cylindrical Nozzle”. In: *Mechanism and Machine Theory* 156 (2021), p. 104136.

[31] S. Kumar and A. Jain. “Design and optimization of a Bernoulli gripper for high-speed pick and place”. In: *International Journal of Advanced Manufacturing Technology* 83 (2016), pp. 1971–1982.

[32] A. Kandemir and H. Caliskan. “Contactless Picking of Objects Using an Acoustic Gripper”. In: *Actuators* 10.4 (2021), p. 70.

[33] David Röthlisberger. “Development and Control of a Standing Wave-Based Acoustic Robot Gripper”. In: *ETH Zürich Bachelor’s Thesis* (2018).

[34] Marco A. B. Andrade et al. “Contactless pick-and-place of millimetric objects using inverted near-field acoustic levitation”. In: *Applied Physics Letters* 116.5 (2020), p. 054104.

[35] Hung Pham and Quang-Cuong Pham. “Critically fast pick-and-place with suction cups”. In: *2019 International Conference on Robotics and Automation (ICRA)*. 2019, pp. 3045–3051. doi: 10.1109/ICRA.2019.8794081.

[36] A. Bicchi and V. Kumar. “Robotic grasping and contact: a review”. In: *Proceedings 2000 ICRA. Millennium Conference. IEEE International Conference on Robotics and Automation. Symposia Proceedings (Cat. No.00CH37065)*. Vol. 1. 2000, 348–353 vol.1. doi: 10.1109/ROBOT.2000.844081.

[37] Domenico Prattichizzo and Jeffrey C. Trinkle. “Grasping”. In: *Springer Handbook of Robotics*. Ed. by Bruno Siciliano and Oussama Khatib. Cham: Springer International Publishing, 2016, pp. 955–988. doi: 10.1007/978-3-319-32552-1_38. url: https://doi.org/10.1007/978-3-319-32552-1_38.

[38] Matthew T. Mason. *Mechanics of Robotic Manipulation*. The MIT Press, June 2001. isbn: 9780262256629. doi: 10.7551/mitpress/4527.001.0001. url: https://doi.org/10.7551/mitpress/4527.001.0001.

[39] Matei T. Ciocarlie and Peter K. Allen. “Data-Driven Optimization for Underactuated Robotic Hands”. In: *Proceedings of the 2010 IEEE International Conference on Robotics and Automation (ICRA)*. Anchorage, AK, USA, 2010, pp. 1292–1299. doi: 10.1109/ROBOT.2010.5509793. eprint: https://roam.me.columbia.edu/sites/default/files/content/papers/icra2010_optimization.pdf. url: https://doi.org/10.1109/ROBOT.2010.5509793.

[40] Lael U. Odhner et al. “A compliant, underactuated hand for robust manipulation”. In: *The International Journal of Robotics Research* 33.5 (2014), pp. 736–752. doi: 10.1177/0278364913514466. eprint: https://arxiv.org/pdf/1301.4394.pdf. url: https://doi.org/10.1177/0278364913514466.

[41] João Bimbo et al. “Teleoperation in Cluttered Environments Using Wearable Haptic Feedback”. In: *2017 IEEE/RSJ International Conference on Intelligent Robots and Systems (IROS)*. Vancouver, BC, Canada, 2017, pp. 3401–3408. doi: 10.1109/IROS.2017.8206180. eprint: https://ieeexplore.ieee.org/stamp/stamp.jsp?arnumber=8206180. url: https://doi.org/10.1109/IROS.2017.8206180.

[42] Carlo Ferrari and John F. Canny. “Planning optimal grasps”. In: *Proceedings 1992 IEEE International Conference on Robotics and Automation* (1992), 2290–2295 vol.3. url: https://api.semanticscholar.org/CorpusID:32592111.

[43] Oricus Semicon Technologies. *Vacuum Relief Tips – Rubber Tips for Die Attach*. https://oricus-semicon.com/products/die-attach/rubber-tips/vacuum-relief-tips/. Accessed: 30 July 2025. 2025.

[44] Kevin M. Lynch and Frank C. Park. *Modern Robotics: Mechanics, Planning, and Control*. 1st. USA: Cambridge University Press, 2017. isbn: 1107156300.

[45] Elon Rimon and Joel Burdick. *The Mechanics of Robot Grasping*. Cambridge University Press, 2019.

[46] Stephen Timoshenko and Sergius Woinowsky-Krieger. “Theory of plates and shells”. In: (1959).

[47] Milan Batista. “New analytical solution for bending problem of uniformly loaded rectangular plate supported on corner points”. In: *The IES Journal Part A: Civil & Structural Engineering* 3.2 (2010), pp. 75–84. doi: 10.1080/19373261003607907. eprint: https://doi.org/10.1080/19373261003607907. url: https://doi.org/10.1080/19373261003607907.

[48] I. E. Roslon. “Probing Nanoscale Forces of Nature in Fluid: From Pneumatics to Biomechanics”. [Online]. Available: https://doi.org/10.4233/uuid:5c3cc4c4-f38a-43ce-851a-8f758769171a. PhD thesis. Delft, The Netherlands: Delft University of Technology, 2023. doi: 10.4233/uuid:5c3cc4c4-f38a-43ce-851a-8f758769171a.

[49] Chih-Hsing Liu, Fu-Ming Chung, and Yuan-Ping Ho. “Topology Optimization for Design of a 3D-Printed Constant-Force Compliant Finger”. In: *IEEE/ASME Transactions on Mechatronics* 26.4 (2021), pp. 1828–1836. doi: 10.1109/TMECH.2021.3077947.

[50] Wenfu Xu et al. “A Compliant Adaptive Gripper and Its Intrinsic Force Sensing Method”. In: *IEEE Transactions on Robotics* PP (Mar. 2021), pp. 1–20. doi: 10.1109/TRO.2021.3060971.

[51] Yilin Liu and Yulong Zhang. “Design and Control of a Novel Compliant Constant-Force Gripper Based on Buckled Fixed-Guided Beams”. In: *IEEE/ASME Transactions on Mechatronics* PP (Oct. 2016), pp. 1083–4435. doi: 10.1109/TMECH.2016.2614966.

[52] Yinyin Su et al. “A High-Payload Proprioceptive Hybrid Robotic Gripper With Soft Origamic Actuators”. In: *IEEE Robotics and Automation Letters* PP (Feb. 2020), pp. 1–1. doi: 10.1109/LRA.2020.2974438.

[53] Yingtian Li et al. “Soft Robotic Grippers Based on Particle Transmission”. In: *IEEE/ASME Transactions on Mechatronics* 24.3 (2019), pp. 969–978. doi: 10.1109/TMECH.2019.2907045.

[54] Zhongkui Wang, Yui Makiyama, and Shinichi Hirai. “A soft needle gripper capable of grasping and piercing for handling food materials”. In: *Journal of Robotics and Mechatronics* 33.4 (2021), pp. 935–943.

[55] Shoufeng Liu et al. “A Two-Finger Soft-Robotic Gripper With Enveloping and Pinching Grasping Modes”. In: *IEEE/ASME Transactions on Mechatronics* 26.1 (2021), pp. 146–155. doi: 10.1109/TMECH.2020.3005782.

[56] Qiujie Lu et al. “An Origami-Inspired Variable Friction Surface for Increasing the Dexterity of Robotic Grippers”. In: *IEEE Robotics and Automation Letters* 5.2 (2020), pp. 2538–2545. doi: 10.1109/LRA.2020.2972833.

[57] Panipat Wattanasiri, Pairat Tangpornprasert, and Chanyaphan Virulsri. “Design of Multi-Grip Patterns Prosthetic Hand With Single Actuator”. In: *IEEE Transactions on Neural Systems and Rehabilitation Engineering* 26.6 (2018), pp. 1188–1198. doi: 10.1109/TNSRE.2018.2829152.

[58] Evelin Villegas et al. “A Vacuum-driven Origami “Magic-ball” Soft Gripper”. In: (Mar. 2019).

[59] Zhenishbek Zhakypov et al. “An Origami-Inspired Reconfigurable Suction Gripper for Picking Objects With Variable Shape and Size”. In: *IEEE Robotics and Automation Letters* PP (June 2018), pp. 1–1. doi: 10.1109/LRA.2018.2847403.

[60] Gareth J Monkman et al. *Robot grippers*. John Wiley & Sons, 2007.

[61] Takeshi Nishida, Yuki Okatani, and Kenjiro Tadakuma. “Development of Universal Robot Gripper Using MRα Fluid”. In: *International Journal of Humanoid Robotics* 13.04 (2016), p. 1650017. doi: 10.1142/S0219843616500171. eprint: https://doi.org/10.1142/S0219843616500171. url: https://doi.org/10.1142/S0219843616500171.

[62] Geonwoo Hwang et al. “Electroadhesion-Based High-Payload Soft Gripper With Mechanically Strengthened Structure”. In: *IEEE Transactions on Industrial Electronics* PP (Jan. 2021), pp. 1–1. doi: 10.1109/TIE.2021.3053887.

[63] Dong Liu et al. “Soft-acting, noncontact gripping method for ultrathin wafers using distributed Bernoulli principle”. In: *IEEE Transactions on Automation Science and Engineering* 16.2 (2018), pp. 668–677.

[64] S Davis, JO Gray, and Darwin G Caldwell. “An end effector based on the Bernoulli principle for handling sliced fruit and vegetables”. In: *Robotics and Computer-Integrated Manufacturing* 24.2 (2008), pp. 249–257.

[65] Dong Liu et al. “Development of a distributed Bernoulli gripper for ultra-thin wafer handling”. In: *2017 IEEE International Conference on Advanced Intelligent Mechatronics (AIM)*. 2017, pp. 265–270. doi: 10.1109/AIM.2017.8014028.

[66] Xin Li and Toshiharu Kagawa. “Theoretical and Experimental Study of Factors Affecting the Suction Force of a Bernoulli Gripper”. In: *Journal of Engineering Mechanics* 140.9 (2014), p. 04014066. doi: 10.1061/(ASCE)EM.1943-7889.0000774. eprint: https://ascelibrary.org/doi/pdf/10.1061/%28ASCE%29EM.1943-7889.0000774. url: https://ascelibrary.org/doi/abs/10.1061/%28ASCE%29EM.1943-7889.0000774.

A

Appendix

A.1. Gripper Classification

Based on the domain of the object size which the gripper has to manipulate, they can be categorised as micro-grippers and standard grippers. Since the medical sensor, which is being handled by the gripper, is millimetric in size, the domain of micro-grippers has been considered as out of scope of this literature study.

Grippers can also be classified based on the principle of actuation, the principle of grasping the object and design configurations. For the current literature survey, it has been decided that the grippers will be classified based on the principle of object grasping. This is done because the primary task of the gripper in the current case study is to pick and place the medical sensor while ensuring minimal gripping to prevent surface damage. Therefore, the following classification tree has been developed to continue an in-depth study of grippers in the literature.

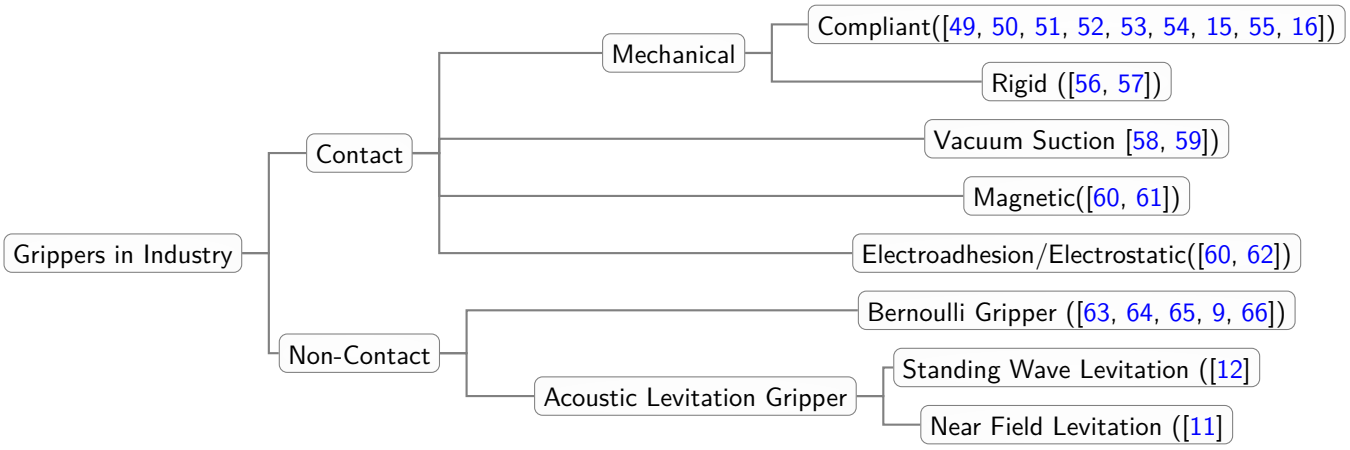

A.2. Example: Wrench Matrix Construction for a Square Chip (Two Contacts)

This example derives the discrete wrench set for a $5\,\mathrm{mm} \times 5\,\mathrm{mm} \times 0.5\,\mathrm{mm}$ chip grasped on its top surface using two corner contacts. Parameters:

$$\mu = 0.3, \quad n_{\text{rays}} = 4, \quad \text{angle} = -90^\circ, \quad F_{\text{norm}} = -0.75\ \mathrm{N}.$$

Step 1: Contact positions and centre of mass

We place the object frame at the *midplane*, so the centre of mass is $\mathbf{c} = (0, 0, 0)$. The (top-surface) contacts are

$$\mathbf{p}_1 = (2.2,\ 2.2,\ 0.25)\,\mathrm{mm}, \qquad \mathbf{p}_2 = (-2.2,\ 2.2,\ 0.25)\,\mathrm{mm}.$$

Relative positions $\mathbf{r}_i = \mathbf{p}_i - \mathbf{c}$ have $r_{1x} = +2.2$, $r_{1y} = +2.2$, $r_{1z} = +0.25$ (mm) and $r_{2x} = -2.2$, $r_{2y} = +2.2$, $r_{2z} = +0.25$ (mm).

Step 2: Normalization factor

$$\|\mathbf{r}_i\| = \sqrt{2.2^2 + 2.2^2 + 0.25^2} = 3.1213 \text{ mm}, \qquad R = \frac{1}{2}\sum_{i=1}^{2} \|\mathbf{r}_i\| = 3.1213 \text{ mm}.$$

Useful ratios:

$$\frac{r_x}{R} = \frac{r_y}{R} = 0.7048, \qquad \frac{r_z}{R} = 0.0801 \quad (\text{for } |r_x| = |r_y| = 2.2 \text{ mm}).$$

Step 3: Contact normal and tangents (angle $= -90°$)

With the code's rule $\mathbf{n}_i = \mathbf{h}\cos\alpha + \hat{\mathbf{z}}\sin\alpha$ and $\alpha = -90°$,

$$\mathbf{n}_i = (0, 0, -1), \quad \mathbf{t}_1 = (1, 0, 0), \ \mathbf{t}_2 = (0, 1, 0).$$

Step 4: Polyhedral friction cone (four rays)

For $\theta_j \in \{0°, 90°, 180°, 270°\}$,

$$\mathbf{f}' = \mathbf{n}_i + \mu(\cos\theta_j\, \mathbf{t}_1 + \sin\theta_j\, \mathbf{t}_2), \quad \mathbf{f} = \frac{\mathbf{f}'}{\|\mathbf{f}'\|} F_{\text{norm}},$$

with $\|\mathbf{f}'\| = \sqrt{1+\mu^2} = 1.0440$. The four force samples (all contacts share these) are

$$\begin{aligned} \theta = 0° &: \ \mathbf{f} = (-0.2155,\ 0,\ 0.7184), \\ \theta = 90° &: \ \mathbf{f} = (0,\ -0.2155,\ 0.7184), \\ \theta = 180° &: \ \mathbf{f} = (0.2155,\ 0,\ 0.7184), \\ \theta = 270° &: \ \mathbf{f} = (0,\ 0.2155,\ 0.7184). \end{aligned}$$

Step 5: Grasp block and wrenches

The torque rows use $(\mathbf{r}_i \times \mathbf{f})/R$, i.e.

$$\frac{[\mathbf{r}_i]_\times}{R} = \begin{bmatrix} 0 & -r_{iz}/R & r_{iy}/R \\ r_{iz}/R & 0 & -r_{ix}/R \\ -r_{iy}/R & r_{ix}/R & 0 \end{bmatrix}.$$

For contact 1: $(r_x, r_y, r_z)/R = (+0.7048, +0.7048, +0.0801)$;
For contact 2: $(r_x, r_y, r_z)/R = (-0.7048, +0.7048, +0.0801)$.

Step 6: Final discrete wrench matrix (two contacts, eight rays)

Columns are ordered by contact then ray: $[(i{=}1, j{=}0°, 90°, 180°, 270°),\ (i{=}2, \dots)]$.

$$\mathbf{W} = \begin{bmatrix} -0.2155 & 0 & 0.2155 & 0 & -0.2155 & 0 & 0.2155 & 0 \\ 0 & -0.2155 & 0 & 0.2155 & 0 & -0.2155 & 0 & 0.2155 \\ 0.7184 & 0.7184 & 0.7184 & 0.7184 & 0.7184 & 0.7184 & 0.7184 & 0.7184 \\ 0.5063 & 0.5236 & 0.5063 & 0.4891 & 0.5063 & 0.5236 & 0.5063 & 0.4891 \\ -0.5236 & -0.5063 & -0.4891 & -0.5063 & 0.4891 & 0.5063 & 0.5236 & 0.5063 \\ 0.1519 & -0.1519 & -0.1519 & 0.1519 & 0.1519 & 0.1519 & -0.1519 & -0.1519 \end{bmatrix}$$

(Units: forces in N; torques are $(\mathbf{r} \times \mathbf{f})/R$ as in the implementation.)

Step 7: Building the complete set

To obtain the full discrete wrench set for more contacts, repeat the per-contact construction above and *append the resulting columns* to $\mathbf{W}$. Under the L1 model the overall discrete set is the union of these columns.

A.3. Pick-and-Place G-code Script

```
G28 ; Home all axes
T6 ; Select Head 7 (tool slot 6)
G0 X250 Y250 Z10 ; Move to initial position
M660 H7 Z0 ; Set tool offset for Head 7

; First chip
G0 X250.0 Y250 Z0.5 ; Move to first chip position
G4 P500 ; Dwell for 500ms to simulate pickup
G0 Z10 ; Raise to safe height
G0 X200 Y200 ; Move to first placement position
G0 Z0.5 ; Lower for placement
G4 P500 ; Dwell for 500ms to simulate placement
G0 Z10 ; Raise to safe height

; Second chip
G0 X250.5 Y250 Z0.5 ; Move to second chip position
G4 P500 ; Dwell for 500ms to simulate pickup
G0 Z10 ; Raise to safe height
G0 X201 Y200 ; Move to second placement position
G0 Z0.5 ; Lower for placement
G4 P500 ; Dwell for 500ms to simulate placement
G0 Z10 ; Raise to safe height

; Third chip
G0 X251.0 Y250 Z0.5 ; Move to third chip position
G4 P500 ; Dwell for 500ms to simulate pickup
G0 Z10 ; Raise to safe height
G0 X202 Y200 ; Move to third placement position
G0 Z0.5 ; Lower for placement
G4 P500 ; Dwell for 500ms to simulate placement
G0 Z10 ; Raise to safe height

; Fourth chip
G0 X251.5 Y250 Z0.5 ; Move to fourth chip position
G4 P500 ; Dwell for 500ms to simulate pickup
G0 Z10 ; Raise to safe height
G0 X203 Y200 ; Move to fourth placement position
G0 Z0.5 ; Lower for placement
G4 P500 ; Dwell for 500ms to simulate placement
G0 Z10 ; Raise to safe height

; Fifth chip
G0 X252.0 Y250 Z0.5 ; Move to fifth chip position
G4 P500 ; Dwell for 500ms to simulate pickup
G0 Z10 ; Raise to safe height
G0 X204 Y200 ; Move to fifth placement position
G0 Z0.5 ; Lower for placement
G4 P500 ; Dwell for 500ms to simulate placement
G0 Z10 ; Raise to safe height

G28 ; Return to home position
```

A.4. MATLAB Script for Wrench Space and Epsilon Metric Analysis

Listing A.1: MATLAB code for grasp_FC_Linf_vs_L1 with centroid metric and 2D visualization of selected subspaces.

```

clc; clear; close all;

%% 1. Normalization model
normChoice = 'L1';  % 'Linf' or 'L1'

%% 2. Grasp parameters
t_pts  = [ 2.2e-3,  2.2e-3, 0.25e-3;
          -2.2e-3,  2.2e-3, 0.25e-3;
           2.2e-3, -2.2e-3, 0.25e-3;
          -2.2e-3, -2.2e-3, 0.25e-3];
angle  = -90 * pi/180;  % tilt for all contacts
mu     = 0.3;           % friction coefficient
F_norm = -0.75;         % nominal normal force magnitude
n_rays = 8;             % rays per friction cone sample

%% 3. Centroid & scale
cen   = mean(t_pts, 1)';
dists = sqrt(sum((t_pts' - cen).^2, 1));
R     = mean(dists);

%% 4. Build primitive wrench sets
primitives = cell(4,1);
for c = 1:4
    r = t_pts(c,:)' - cen;                    % position relative to centroid
    v = -r;
    if norm(v)<1e-12
        v = [0;0;1];
    end % fallback normal
    h = v / norm(v);
    n1 = h * cos(angle) + [0;0;1] * sin(angle);
    n1 = n1 / norm(n1);
    if abs(n1(3)) < 1
        t1 = cross([0;0;1], n1); t1 = t1 / norm(t1);
        t2 = cross(n1, t1);    t2 = t2 / norm(t2);
    else
        t1 = [1;0;0]; t2 = [0;1;0];
    end
    % grasp matrix G_i with centroid & normalization
    G_i = [ eye(3);
            [  0,  -r(3),  r(2);
              r(3),    0, -r(1);
             -r(2),  r(1),    0 ] / R ];
    % sample friction cone
    thetas = linspace(0, 2*pi, n_rays+1);
    thetas(end) = [];
    Wc = zeros(6, n_rays);
    for j = 1:n_rays
        fdir    = n1 + mu * (cos(thetas(j))*t1 + sin(thetas(j))*t2);
        funit   = (fdir / norm(fdir)) * F_norm;
        Wc(:,j) = G_i * funit;
    end
    primitives{c} = Wc;
end

%% 5. Optional suction wrench
suction = zeros(6,1);
suction(3) = F_norm;

%% 6. Assemble overall wrench set Wset
if strcmp(normChoice,'Linf')
    Wset = primitives{1};
    for c = 2:4
        Wset = minkSum(Wset, primitives{c});
    end
    Wset = minkSum(Wset, suction);
else  % 'L1'
    allW = [primitives{:}, suction];
    U    = unique(allW.', 'rows', 'stable');
```

```
    Wset = U.';
end

%% 7. Visualization of 3D subspaces and 2D projections
nlabels   = {'Fx','Fy','Fz','Tx','Ty','Tz'};
subspaces = { [1,2,3], [4,5,6], [5,6,3] };
names     = { 'FxFyFz',   'TxTyTz',   'FzTxTy' };
pairs     = [1 2; 1 3; 2 3];

for k = 1:numel(subspaces)
    idx = subspaces{k};
    W3  = Wset(idx, :);
    % compute   in 3D via convhulln
    P = W3.';
    if size(P,1) >= 4
        try
            K = convhulln(P);
        catch
            P = P + 1e-12 * randn(size(P));
            K = convhulln(P);
        end
        dmin = inf(size(K,1),1);
        for f = 1:size(K,1)
            tri      = P(K(f,:), :);
            normal_f = cross(tri(2,:)-tri(1,:), tri(3,:)-tri(1,:));
            dmin(f)  = abs(dot(normal_f, tri(1,:))) / norm(normal_f);
        end
        eps3 = min(dmin);
    else
        eps3 = 0;
    end
    fprintf('%s   = %.4f\n', names{k}, eps3);
    % 3D scatter + hull + sphere
    figure('Name',names{k}); hold on; grid on; axis equal;
    scatter3(P(:,1), P(:,2), P(:,3), 20, 'filled');
    try
        K3 = convhull(P(:,1), P(:,2), P(:,3));
        trisurf(K3, P(:,1), P(:,2), P(:,3), 'FaceAlpha',0.1, 'EdgeColor','k',
            'FaceColor','flat', 'FaceVertexCData',P(:,3));
        colormap(jet);
    catch
    end
    if eps3 > 0
        [sx,sy,sz] = sphere(24);
        surf(eps3*sx, eps3*sy, eps3*sz, 'FaceAlpha',0.3, 'EdgeColor','none',
            'FaceColor','r');
    end
    xlabel(nlabels{idx(1)}); ylabel(nlabels{idx(2)}); zlabel(nlabels{idx(3)});
    view(45,30);
    hold off;
    % 2D projections
    for p = 1:size(pairs,1)
        a   = pairs(p,1);
        b   = pairs(p,2);
        pts = W3([a,b], :);
        figure('Name',[names{k} ' ' nlabels{idx(a)} '-' nlabels{idx(b)}]);
        scatter(pts(1,:), pts(2,:), 20, 'filled'); hold on; grid on; axis equal;
        k2 = convhull(pts(1,:)', pts(2,:)');
        plot(pts(1,k2), pts(2,k2), 'k-', 'LineWidth',1);
        t  = linspace(0, 2*pi, 200);
        plot(eps3*cos(t), eps3*sin(t), 'r-', 'LineWidth',1.5);
        xlabel(nlabels{idx(a)}); ylabel(nlabels{idx(b)});
        hold off;
    end
end

%% Minkowski-sum function
function R = minkSum(A, B)
    [~,nA] = size(A);
    [~,nB] = size(B);
    R = zeros(size(A,1), nA*nB);
```

```
    id = 1;
    for i = 1:nA
        for j = 1:nB
            R(:,id) = A(:,i) + B(:,j);
            id = id + 1;
        end
    end
end
```